UNIVERSITY OF OKLAHOMA
GRADUATE COLLEGE

EXAMINING THE CHARACTERISTICS AND EVOLUTION OF TEMPERATURE WHIPLASH EVENTS IN THE US SOUTHERN PLAINS

A THESIS
SUBMITTED TO THE GRADUATE FACULTY
in partial fulfillment of the requirements for the
Degree of
MASTER OF SCIENCE

By

KATHERINE GIANNAKOPOULOS
Norman, Oklahoma
2024

EXAMINING THE CHARACTERISTICS AND EVOLUTION OF TEMPERATURE WHIPLASH EVENTS IN THE US SOUTHERN PLAINS

A THESIS APPROVED FOR THE
SCHOOL OF METEOROLOGY

BY THE COMMITTEE CONSISTING OF

Dr. Jason Furtado (Chair)

Dr. Elinor Martin

Dr. Kathleen Pegion

Acknowledgements

To begin, I would like to thank my advisor, Dr. Jason Furtado, and my committee members, Dr. Elinor Martin and Dr. Kathy Pegion, for their guidance throughout this project. It has been a pleasure to work alongside you all, and you have elevated my skills as a scientist. Additionally, I would like to thank my office mates, Ollie Millin and Dr. Ty Dickinson, for their endless support over the last 2 years. Not only were they willing to answer any questions I had from coding to travel logistics, but our informal research chats sparked many ideas for this thesis.

I completed both my undergraduate and graduate studies at the University of Oklahoma. Throughout my 6 years in Norman, I have had the pleasure of interacting with most of the School of Meteorology's faculty and staff. Thank you for crafting me into the scientist I am today by being dedicated to teaching, inspiring me, and letting me work alongside you. I have truly cherished my time in Oklahoma because of everyone in the National Weather Center.

To all my graduate school friends and the Applied Climate Dynamics group, I would not have been able to reach this point without you. Your advice and support, academically and beyond, has been unrivaled. Thank you for also helping me maintain a work-life balance, which can be extremely difficult in graduate school. You have all made this experience so special, and I will miss you dearly.

To my mom, dad, and brother, thank you. Thank you for supporting my dream of being a meteorologist since the 2nd grade. Whether that was driving me to the beach during a blizzard for my senior project, or buying me a weather station as a Christmas present, you've helped keep this passion alive. Thank you for allowing me to follow my dreams no matter where they take me, while also keeping our close bond and providing an endless amount of love. None of this would have been possible without you and I can't thank you enough.

Lastly, I would like to thank Oklahoma EPSCoR and NSF for supporting my work as a part of the S3OK project. This work is funded by NSF Grant No. OIA-1946093. Thank you for your interest in my project!

Table of Contents

List Of Tables

List Of Figures

Abstract

Rapid extreme temperature swings, termed "temperature whiplashes", can lead to significant and intense socioeconomic impacts. Few studies have considered temperature whiplashes over global, continental, or other large domains. These analyses suggest that certain locations within the domain may experience greater temperature swings, one being the United States Southern Plains. By selecting a specific area and considering temperature whiplashes on a regional scale, skillful, long-lead prediction of and adaptation for these events may be improved. This study focuses on defining and characterizing temperature whiplash events in the Southern Plains region of the United States, specifically during the winter months (December-February). Two types of whiplashes are defined: the hot-to-cold and cold-to-hot. Using the European Centre for Medium-Range Weather Forecasts' Fifth Reanalysis (ERA5) from 1950-2023, the Temperature Swing Index is calculated and area-averaged across the Southern Plains. Days where the Temperature Swing Index exceeds the 90th percentile are termed "high swing days" (HSD). Temperature whiplash events are selected by examining each HSD, and considering the longevity and persistence of the overall temperature trend and the signs of the temperature anomalies up to 4 days before and after the HSD. This definition yields 45 anomalously hot-to-cold whiplash events and 14 cold-to-hot whiplash events. Trends of the HSDs and whiplash events reveal increases in frequency since the 1990s. Composites of the geopotential height field at multiple pressure levels and lags illustrate large-scale atmospheric evolutions and key features, like atmospheric blocking or amplified wave trains, that could enhance long range prediction. Additionally, stratospheric-tropospheric interactions such as wave reflection are identified as a possible precursor to these events. By establishing the characteristics of temperature whiplash events and their precursors, there is the opportunity to improve predictions of these extreme events and determine how they may change in a changing climate.

Chapter 1

Introduction

Extreme weather events can cause significant socioeconomic impacts on energy, agriculture, and transportation. The Intergovernmental Panel on Climate Change (IPCC) Sixth Assessment reported that on a global scale, the number of warm extremes are increasing, while cold extremes are decreasing. These trends have been exacerbated by human influences, like increased greenhouse gas emissions (IPCC 2023). Heavy rainfall, increased tropical cyclone strength, and compound events like heat/drought and fire weather have increased in frequency and intensity, and are projected to continue increasing in the future climate (IPCC 2023).

Extreme temperature variability in particular is becoming a growing peril in North America. Recent research has found that from 1950-2019, the trend of the 2-day temperature change magnitude has increased globally, however from 1985 onward this trend has increased significantly, growing from a decadal z-score of 0.0086 to 0.0104 (Lee 2022). Model experiments also reveal that temperature variability is increasing in the low to mid-latitudes, possibly as a result of Arctic Amplification, where the Arctic warms at a faster rate than the mid-latitudes (Cohen 2016; Francis and Vavrus 2012; Cohen et al. 2014). Climate modes also have the potential to drive temperature variability in the United States. For example, the El Niño Southern Oscillation (ENSO), a climate pattern driven by fluctuations in sea surface temperatures in the equatorial Pacific Ocean, notably impacts temperature patterns across the US, leading to anomalously cold temperatures in the southern US during a La Niña (i.e., the

negative phase or cold episode of ENSO) (Higgins et al. 2002; Meehl et al. 2007; Yang et al. 2022). Atmospheric modes such as the Pacific North American Pattern and North Pacific Oscillation, both related to pressure anomalies over the Pacific Ocean and North America, can also lead to temperature fluctuations in the United States (Cellitti et al. 2006; Yang et al. 2022; Grise et al. 2013). On a subseasonal scale, the Madden-Julian Oscillation (MJO), an eastward propagating area of enhanced and suppressed convection in tropical Indian and western Pacific Oceans, leads to temperature and precipitation differences across the United States, acting as a source of diabatic heating and affecting the jet stream, storm tracks, and climate modes through Rossby wave dispersion (Zheng et al. 2018; Lin 2015; Grise et al. 2013; Moon et al. 2011).

Prediction skill of extreme events is still lacking, especially in the subseasonal-to-seasonal (S2S) range (2 weeks to 2 months), due to complexities of these events (Vitart and Robinson 2018). Robertson et al. (2015) explains how forecasts of the MJO have improved, but low ensemble spreads are leading to overconfident models. However, having skillful forecasts within this time frame is beneficial, as it allows for preemptive adaptations (Coughlan de Perez et al. 2016; Vitart and Robertson 2018). Atmospheric mechanisms like climate modes and atmospheric blocking, defined as enhanced ridges that lead to meridionally-dominated flow (Kautz et al. 2022), vary on the S2S timescale and can be utilized to improve S2S prediction of extremes if they themselves can be skillfully forecasted (Robertson et al. 2015). North American winter weather regimes, which represent anomalous atmospheric circulations beyond the weather timescale, present an optimal framework to examine subseasonal variability due to their persistent nature and usual transitions (Charlton-Perez et al. 2018; Lee et al. 2019; Millin et al. 2022). These regimes have been associated with certain stratospheric polar vortex (SPV) states (Charlton-Perez et al. 2018; Lee et al. 2019), stratosphere-troposphere interactions, surface temperature responses (Messori et al. 2022; Millin et al. 2022; Molina

et al. 2023), and modulation of extreme precipitation and storm tracks (Robertson and Ghil 1999; Amini and Straus 2019; Molina et al. 2023). Utilizing a weather regime approach offers potential advancement of S2S extreme event forecasts, especially in the wintertime when both the stratospheric variability is the greatest and the influence of the tropics on the extratropics is more pronounced (Lee et al. 2019; Molina et al. 2023).

There are various extreme weather types during the Northern Hemisphere winter, including cold air outbreaks (CAOs) and winter warm spells. CAOs are often driven by Arctic phenomena, like a weaker SPV causing a southern migration of the polar jet stream (Francis et al. 2009; Francis and Vavrus 2012; Cohen et al. 2021). In extreme cases, the SPV can become so warm and weak that a Sudden Stratospheric Warming (SSW) occurs, reversing the direction of the zonal wind from westerlies to easterlies (Baldwin and Dunkerton 2001; Charlton and Polvani 2007). North Pacific ridges which can develop a blocking pattern near and over Alaska act as both a precursor and concurrent atmospheric feature for a North American CAO (Loikith and Broccoli 2012; Westby and Black 2015; Millin et al. 2022). Recent research indicates that stratospheric wave reflection and wave breaking, which occur due to tropospheric Rossby wave interactions with the stratosphere also lead to these cold periods (Ding et al. 2023; Matthias and Kretschmer 2020; Messori et al. 2022; Millin et al. 2022).

Winter warm spells are not researched as extensively as CAOs, however analyses have shown that winter warm spells are often collocated with positive geopotential height anomalies over the impacted region, with the most intense anomalies occurring around 250-hPa (Tomczyk et al. 2019; Francis and Vavrus 2012). The 250-hPa geopotential height anomalies were present up to 9 days before the winter warm spell, suggesting extended range prediction of these events (Tomczyk et al. 2019). Warm spells during other seasons follow similar patterns. They are characterized by an enhanced Rossby wave train, an atmospheric block, and clear skies (Domeisen et al.

2023; Francis and Vavrus 2012). A new study focusing on 2 winter warm spells in the Southern Great Plains concluded that the Alaskan ridging weather regime contributed to the winter warm spells, as well as higher than average latent heat fluxes over the Southwestern Great Plains and sensible heat fluxes over the Southeastern Great Plains (Grace et al. 2024).

In recent studies a new weather extreme has been proposed: "weather" or "temperature" whiplash. Temperature whiplashes occur when surface temperatures rapidly transition from a persistent and anomalous temperature pattern to its opposing temperature extreme. For example, in December 2013, Oklahomans experienced temperatures up to 15°F above the climatological mean in Norman, Oklahoma between December 16-19 (Mesonet 2024). However, this pattern abruptly shifted on December 20 with the emergence of a strong winter storm that plummeted temperatures in Norman up to 17.6°F below normal from December 21-24 (Mesonet 2024). Additionally, between December 20-22, Oklahoma received up to an inch of ice across the state (NWS 2013). Many Oklahomans were out of power, with Oklahoma Gas and Electric reporting 8950 power outages as of 10pm on December 21st, 2013 (News6 2013). Power outages when temperatures are substantially below normal pose a threat to human health, including an increased risk of hospitalizations when a power outage is paired with a cold event or ice storm, and can have impacts on health up to a week following the outage (Lin et al. 2021). However, temperature whiplashes, which contain these strong temperature anomalies, are only recently gaining media and research attention, and require further exploration at the foundational level.

Defining temperature whiplash events still remains a challenge. When considering a large domain, Francis et al. (2021) defined temperature whiplashes as "transitions from one persistent large scale regime to a distinctly different one" through using self-organizing maps on anomalies from the 500-hPa geopotential height field. Francis

et al. (2021) defined "long duration events" (LDE), which are times when the synoptic patterns remained in the same node for 4 or more days. A "weather whiplash" occurred when the two days following an LDE were notably different from the LDE (Francis et al. 2021). Considering 500-hPa geopotential heights anomalies is effective when considering a large continental scale, however it becomes difficult to use a similar methodology when analyzing temperature whiplash events on a smaller regional domain. The methodology overlooks local temperature variations by focusing on overall temperature fluctuations across a larger area. As a result, regional responses to temperature whiplash events becomes difficult.

Utilizing a smaller domain suggests a different approach. Casson et al. (2019) defines "weather whiplash" as periods in the US Northeast when the air temperature oscillates above and below freezing. This criterion was selected as a phase change from liquid to solid precipitation leads to more drastic human impacts (Casson et al. 2019). An impact-based approach allows for enhanced local adaptations, but is difficult to utilize for multiple regions. For example, in Oklahoma an "anomalous cold event" does not always mean below 32°F. Additionally, resilience to cold weather varies between regions, thus it cannot be assumed that adaptation would be the same for all regions. As such, a regional methodology can aid in domain-specific precursors, as atmospheric precursors for a temperature whiplash event in the Northeast US may vary from those in the US Southern Plains, for example.

Temperature whiplashes vary from CAOs or heat waves, as they may not have as intense or persistent temperature anomalies. Additionally, prediction of temperature swings are not directly related to the prediction of surface temperatures. Yang et al. (2022) found the Temperature Swing Index (TSI), a metric describing the standard deviation temperatures between 2 days, was related to the gradient of surface air temperature, not the temperatures themselves, leading to unique connections between

the TSI, climate modes, and their atmospheric drivers. The few studies that explore temperature whiplash found that on large scales it occurred most frequently when anomalous troughing or ridging dominated the high latitudes, "meridionally oriented dipoles" of 500-hPa height anomalies were present (Francis et al. 2021), or there was a warmer North Atlantic and "North Pacific Oscillation-like" circumglobal Rossby wave (Shuangmei and Congwen 2023). However, regional-specific temperature whiplash precursors, as well as the atmospheric patterns associated with them remain unknown.

This thesis aims to develop a novel, regional methodology to explain temperature whiplash in the context of the US Southern Plains. However, the same methodology can be utilized over other regional domains as well. We will also investigate the trends in temperature whiplash events to understand how these may change in the future. Lastly, the temperature whiplash atmospheric circulations, as well as their precursors are explored. While modeling of these temperature whiplashes is beyond the scope of this thesis, it is anticipated that the results of this study can be utilized in the future to model these extremes, especially in the context of S2S prediction. The research questions of this study are:

1. How do we define temperature whiplash events on a regional scale (i.e. the US Southern Plains)?

2. What atmospheric circulation patterns lead to temperature whiplash events in the US Southern Plains?

3. How do the atmospheric circulation patterns associated with temperature whiplash events evolve?

4. How have the frequency and magnitude of temperature whiplashes changed over time?

Since temperature whiplash events by definition have a period of warm and cold extremes, we hypothesize that atmospheric features connected to CAOs and winter warm spells, like atmospheric blocking and stratosphere-troposphere interactions, are also important for temperature whiplashes. Additionally, we hypothesize that the US Southern Plains may have different precursors than those that have been identified on a large scale since local temperature variations will be considered with this methodology.

Chapter 2

Data & Methods

2.1 Reanalysis Data

The main data source for this project was the European Centre for Medium-Range Weather Forecasts' Fifth Global Reanalysis (ERA5) (Hersbach et al. 2020). For all the variables in this study, 6-hourly data on a 0.5°x0.5°grid was used from 1950-2023, including only December, January, and February to focus on wintertime variability. This season was selected so we could build upon the existing framework established in Yang et al. (2022) which focused wintertime temperature variability. Table 1 lists these variables and in what statistical analysis they were used. The analyses will be defined in later chapters.

Analysis	Variables
Temperature Swing Index	2m Temperature
Height Composites	Geopotential Height: 500-hPa, 50-hPa, 10-hPa
Wave Activity Flux (vertical component)	100-hPa Pressure, 100-hPa V-Wind,100-hPa U-Wind, 100-hPa Geopotential Height
Reflection Index	100-hPa Temperature, 100-hPa V-Wind

Table 2.1: The ERA5 variables used in this study by analysis

The height fields, wave activity flux, and Reflection Index were daily-averaged prior to analysis.

2.2 Defining Temperature Whiplash Events

2.2.1 Temperature Swing Index

Since temperature whiplash events are a relatively new area of research, there are few methodologies upon which to build a definition. While we considered multiple methodologies, the method used by Yang et al. (2022) fit the needs of our study. In their work, the TSI was derived from the Extratropical Storm Track Index (ESTI), which is defined as the "the seasonal standard deviation of the 24-h difference filtered 6-hourly sea level pressure (SLP)":

$$ESTI = \sqrt{\frac{1}{N-1}\sum_{n=1}^{N}[SLP(n+24hr) - SLP(n)]^2} \tag{2.1}$$

The ESTI has been commonly used in past literature to examine seasonal-to-subseasonal extratropical storm tracks (Zheng et al. 2021; Yang et al. 2015, 2018). To derive the TSI, Yang et al. (2022) replaced SLP with surface air temperature (SAT). The equation for the TSI is defined as:

$$TSI = \sqrt{\frac{1}{N-1}\sum_{n=1}^{N}[SAT(n+24hr) - SAT(n)]^2} \tag{2.2}$$

where n is the 6-hourly time step and N is the number of time steps in a 24-hour period (in this analysis $N = 4$).

Through considering the synoptic eddy temperature perturbations in the lower troposphere, Yang et al. (2022) found that the TSI is proportional to the product of the eddy heat flux and the mean temperature gradient. This is an important finding, as the TSI is not only directly related to the change in SAT itself, but rather the gradient.

This relationship means that the patterns of TSI are likely to be different than those of SAT.

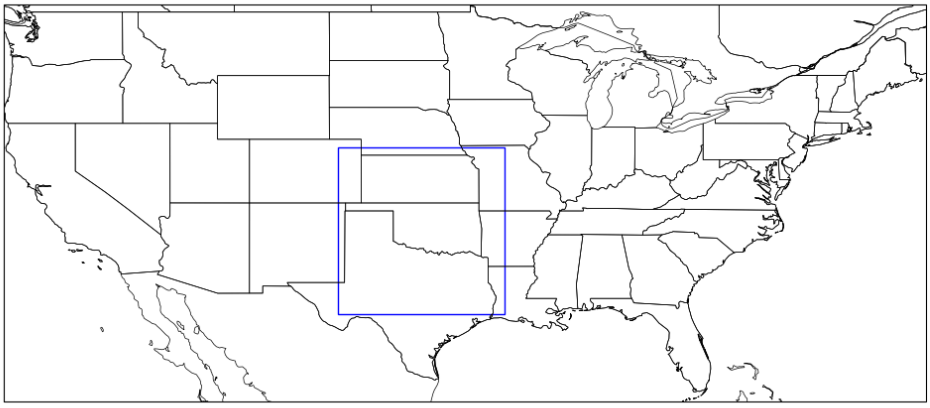

Figure 2.1: Southern Plains domain for this study (blue box).

To define temperature whiplash events, the TSI was calculated at each grid point within the Southern Plains domain, defined between 30-40.5°N and 103.5-93°W to include all of Oklahoma and Kansas while also minimizing ocean data points over the Gulf of Mexico, every 6 hours between 1950-2023 over the DJF period. The Southern Plains was selected as it was shown in Yang et al. (2022) to be an area of climatologically higher temperature swings. The domain of this study is shown in the black box in Figure 2.1. These values were then area-averaged to get one "Southern Plains TSI" value for each day. Days when the Southern Plains TSI value was greater than the 90th percentile of the DJF Southern Plains TSI were termed "High Swing Days" (HSDs). The 90th percentile was chosen to select only the most extreme temperature swings. The temperature trend and anomalies were then considered to identify two different types of whiplashes: hot-to-cold and cold-to-hot. For all of the lag composites presented in this analysis, lag day zero refers to the HSDs of the whiplash events. Note that anomalies in this study are calculated using a 1991-2020 daily-mean climatology of the

given variable. The hot-to-cold whiplash consists of an anomalously warm pattern that transitions to an anomalously cool pattern following the temperature swing.

To be considered a **hot-to-cold** whiplash, the:

- Area-averaged temperature trend from 4 days before to 4 days after HSD must be **less than -1°C/day**.
- Area-averaged temperature anomalies for the 4 days prior to HSD must be **positive**.
- Area-averaged temperature anomalies for the 4 days following HSD must be **negative**.

The cold-to-hot whiplash is the opposite pattern, transitioning from a cold spell to a warm spell. To be considered a **cold-to-hot** whiplash, the:

- Area-averaged temperature trend from 4 days before to 4 days after HSD must be **greater than 1°C/day**.
- Area-averaged temperature anomalies for the 4 days prior to HSD must be **negative**.
- Area-averaged temperature anomalies the 4 days following HSD must be **positive**.

With these definitions, we identified 45 hot-to-cold whiplashes and 14 cold-to-hot whiplashes from 1950-2023. Possible explanations for the difference in sample size will be discussed in Chapter 3.

The 4-day lead time and lag time was selected for multiple reasons. Francis et al. (2021) utilized a 4-day period to define long-duration events, defined as cases where

the upper air patterns remained in the same node of the self-organizing map matrix based on 500-hPa geopotential height anomalies. While our methodology does not use self-organizing maps nor define events based on their upper-air patterns, this length of time for enough persistent temperature patterns also led to distinct 500-hPa geopotential height patterns. Additionally, when testing multiple lead and lag times, 4 days produced a relatively large sample size for our composites. When increasing the same lead and lag to 5 days, there was a drastic decrease in the sample size, but when increasing it to 3, the number of cases were about the same.

2.3 Stratospheric Influences

When considering possible mechanisms for wintertime temperature shifts, variability in the stratospheric polar vortex can drive changes in the tropospheric flow (Baldwin and Dunkerton 2001; Charlton and Polvani 2007; Cohen et al. 2021). While tropospheric Rossby waves propagate horizontally, they also propagate in the vertical. In such cases, they have the ability to interact with and deform the polar vortex. To consider the vertical propagation of these waves, the vertical component of the Plumb Wave Activity Flux (WAFz; Plumb 1985) was used. WAFz is defined as:

$$\mathbf{F}_s = p\cos\phi\left(\frac{2\Omega\sin\phi}{S}\left[v'T' - \frac{1}{2\Omega a\sin 2\phi}\frac{\partial\left(T'\Phi'\right)}{\partial\lambda}\right]\right) \tag{2.3}$$

where a is the Earth's radius, Φ is geopotential, p is pressure/1000-hPa, λ is longitude, ϕ is latitude, u is the zonal wind, v is the meridional wind, T is the temperature, and S is the static stability. The prime notation indicates the perturbations from the zonal mean. Static stability is calculated as:

$$S = \frac{\partial\hat{T}}{\partial z} + \frac{K\hat{T}}{H} \tag{2.4}$$

where K is dry air gas constant divided by the specific heat at constant pressure, z is height, and $H = 8300$m, the atmospheric scale height. Additionally, the carat notation represents an aereal average north of 20°N. To account for only planetary-scale waves, which impact the SPV the most, WAF was filtered for wavenumbers 1-3.

When vertically propagating Rossby waves encounter the polar vortex, they can either break or reflect. While both wave breaking and wave reflection can lead to CAOs, wave breaking CAOs are more tropospheric-driven; they lead to anticyclonic blocking that disrupts the synoptic flow and SPV due to an intrusion of air with a lower potential vorticity (Millin and Furtado 2022; McIntyre and Palmer 1983). Consequently, wave reflection occurs when increased curvature of the vertical and meridional profiles of the zonal-mean zonal wind create a reflecting surface and meridional waveguide at high latitudes (Kodera et al. 2008; Perlwitz and Harnik 2003; Matthias and Kretschmer 2020). While this also leads to enhanced blocking and CAOs in North America, this phenomenon is more stratospheric-driven (Matthias and Kretschmer 2020; Messori et al. 2022; Millin et al. 2022). To explore wave reflection related whiplash events, we use the Reflection Index (RI) from Matthias and Kretschmer (2020). RI is defined as:

$$RI = (v'T')^*_{Siberia} - (v'T')^*_{Canada} \tag{2.5}$$

where *(v'T')* is the meridional eddy heat flux at 100-hPa, the prime notation indicates perturbations from the zonal mean, and the asterisk denotes area-averaged standardized anomalies.

When using this index to examine wave reflection, positive $v'T'$ over Siberia and negative $v'T'$ over Canada leads to a positive RI value. To be considered reflection, this study follows Messori et al. (2022) and defines reflection as an RI value of greater than 1. Messori et al. (2022) also imposes a 10 day reflection period to be considered a

"reflection event", however as will be discussed in Chapter 4, this is not a criteria that was used in this study.

2.4 North American Winter Weather Regimes

To consider the impact of the SPV on tropospheric flow, weather regimes are advantageous. North American winter weather regimes provide a unique approach to analyzing tropospheric patterns, and offer considerable value to prediction on a subseasonal-to-seasonal time scale (Lee et al. 2019). Additionally, certain regimes are linked to CAOs (Lee et al. 2019; Millin et al. 2022). To consider these regimes in the context of temperature whiplash, we use the database from Millin et al. (2022). To create this database, Millin et al. (2022) used k-means clustering on the 12 leading principal component time series of the 500-hPa linearly detrended geopotential height anomalies over North America between 1950 and 2021. This database includes the November-March months, and was further expanded to include the 2022 and 2023 winter seasons. As a result, they defined 5 regimes, adding an additional regime from Lee et al. (2019): the Arctic High, Arctic Low, Alaskan Ridge, Pacific Trough, and West Coast Ridge. The spatial patterns for each regime are shown in Figure 2.2. Note that the frequency of occurrences percentages may vary slightly with the inclusion of 2022-2023 data.

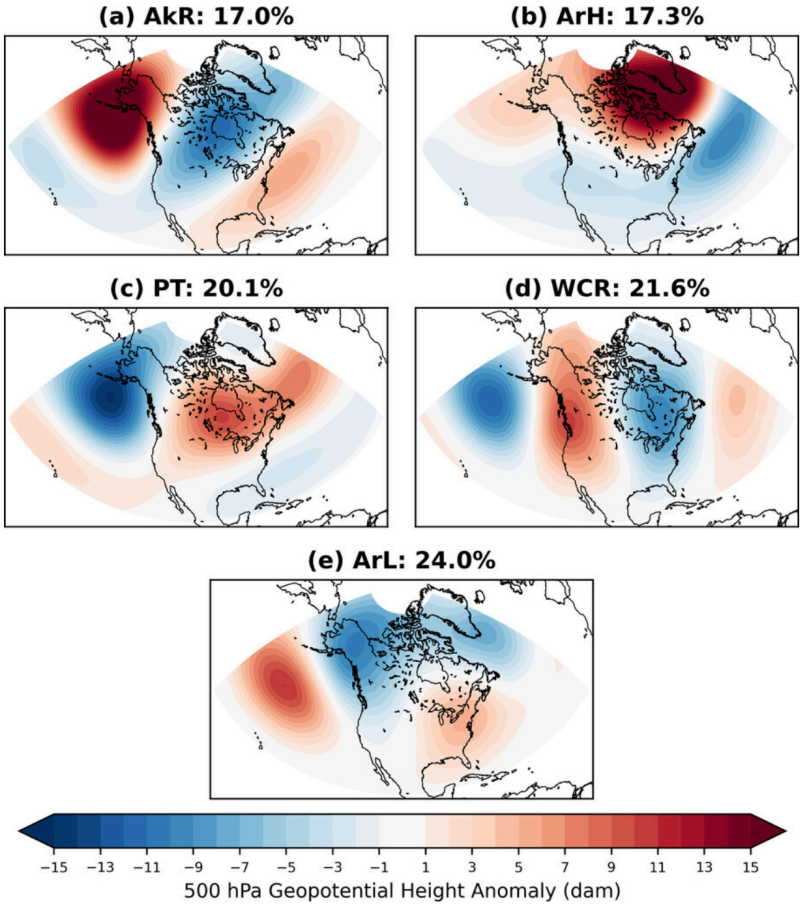

Figure 2.2: Figure 4 of Millin et al. (2022) illustrating the 5 weather regime clusters.

2.5 Statistical Significance Testing

To determine statistical significance in this study, we use 5000-sample bootstrapping without replacement and choose $p < 0.05$ as our threshold for significance. Random samples were selected from the 1950-2023 dataset, and locations of significance are located by hatching on spatial maps and red dots on time series plots in the following chapters.

Chapter 3

Whiplash Trends

3.1 HSD Trends

We begin by exploring HSDs in the US Southern Plains. Defined as the 90th percentile of all the Southern Plains TSI values, 659 HSDs were identified. Figure 3.1 presents the full distribution of the TSI magnitudes and Figure 3.2 displays the distribution of the TSI magnitudes over the HSDs. Since the whiplash criteria only considers TSI days greater than the 90th percentile, the distribution of both the early (1950-1985) and latter (1986-2023) time series were unsurprisingly right-skewed. Additionally, the latter half of the dataset has lower TSI values than the earlier half; however, the right tail also extends further than the earlier half of the time series, possibly indicating more extreme swings in the latter period. Overall though, the Kolmogorov-Smirnov test revealed that there is not a statistically significant difference between the two halves of the time series ($p = .404$).

One disadvantage of selecting the HSDs using the 90th percentile is the number of swings in each whiplash type. Since there was no criteria specifying the direction of the swing, the number of hot-to-cold and cold-to-hot swings are not equal. Of the 659 HSDs, 253 (38%) had a positive swing (a cold-to-hot swing) and 406 (62%) had a negative swing (a hot-to-cold swing). However, $\sim$5.5% of cold-to-hot swings met the whiplash criteria, whereas $\sim$11% of the hot-to-cold swings met the whiplash criteria.

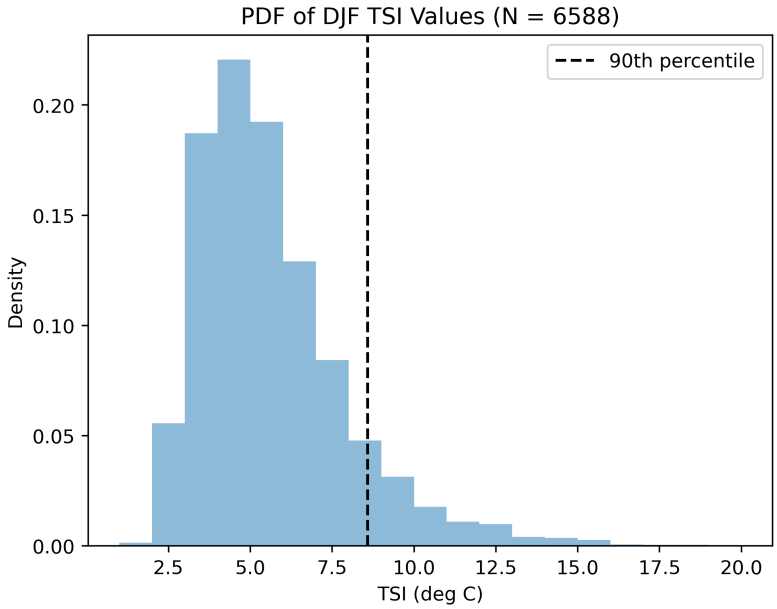

Figure 3.1: PDF of the daily TSI (°C) from December-January 1950-2023. The black dashed line represents the 90th percentile.

Not only are there more hot-to-cold swings in the 90th percentile, but the criteria for the hot-to-cold swings is also met at a rate of over double that of the cold-to-hot whiplashes. Possible reasoning for this will be discussed in the coming chapters.

Figure 3.3 illustrates the frequency and magnitude of HSDs by decade. The frequency of HSDs increased from the 1950s to 1970s, before declining and hitting a minimum in the 1990s, with 69 HSDs occurring. However, since the 1990s there has been an increase in the number of HSDs. In the 2010s, 103 HSDs occurred, the most in a decade. Even so, the 2020s have the potential to exceed this. With 11 winter months occurring so far in the 2020s, this averages about 4 HSDs a month. At this rate, there could be around 120 HSDs over this decade, far surpassing the number of HSDs in the 2010s. This emphasizes the need for further research into temperature whiplashes, as this increase could lead to more potential whiplash events. In response, greater health impacts, power outages, and infrastructure damage could be expected.

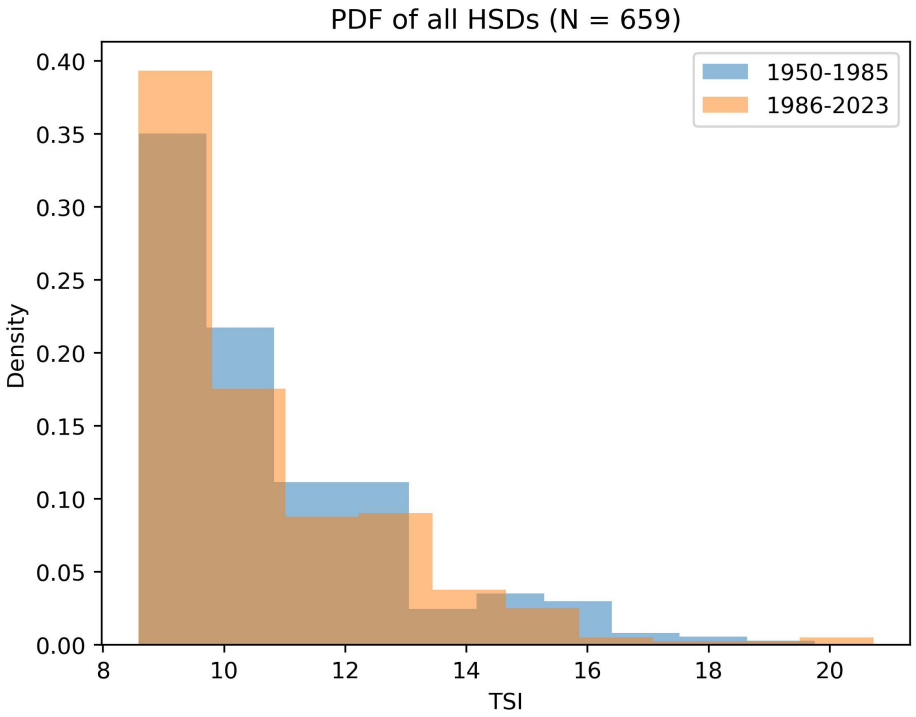

Figure 3.2: PDF of the TSI (°C) for HSDs with the time series split in half. Blue shading represents the early half of the time series (1950-1985) and orange shading represents the latter half (1986-2023).

Considering the TSI magnitude by decade, there is minimal change. While there was a general decrease from the 1950s to the 1990s, the time series' absolute minimum in the 2010s makes depicting any trends difficult. Following the 1990s, there was an increase of 0.24°C, but the TSI magnitude dropped to previous values the following decade. While it appears the 2020s had a higher TSI magnitude than the 2010s, there was no marked increase like there was for the HSD frequency (Figure 3.3a). Overall, while the HSD frequency has increased since the 1990s, the magnitude does not indicate notable changes.

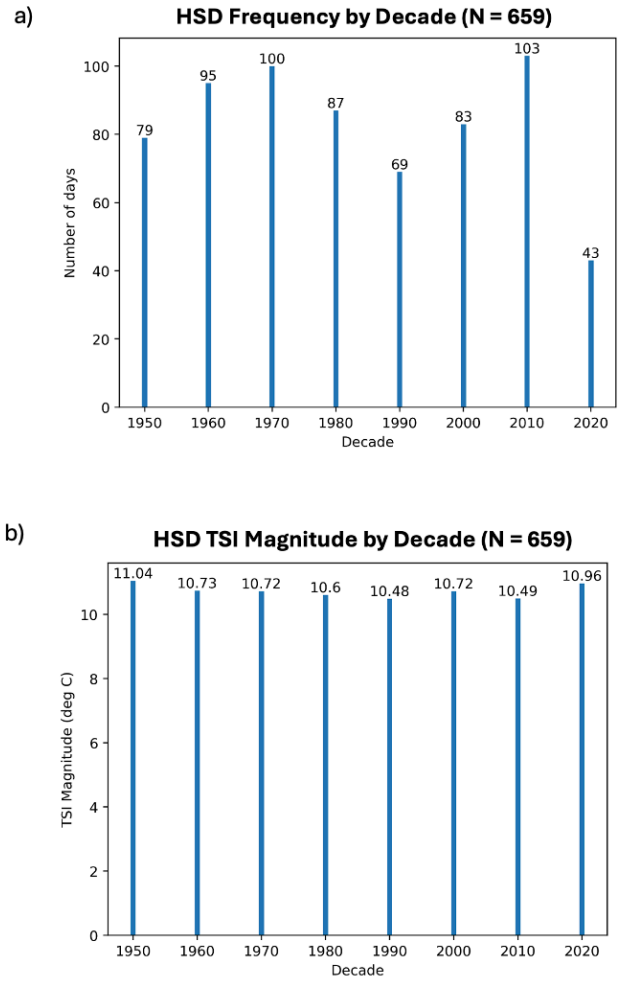

Figure 3.3: (a) Average frequency (days) and (b) average magnitude (°C) of HSDs in the Southern Plains by decade (N = 659).

Next, we investigate the characteristics of the top 5% of HSDs (N = 33; termed "extreme HSDs" herein, Figure 3.4). Out of the 33 days, the highest frequency of extreme HSDs were in the earlier half of the time record, with 8 in the 1950s and 6 in the 1960s. A possible reason for this increase is the anomalous seasonal temperatures in this period. Figure 3.5 displays the average DJF temperatures for the 8 years with the greatest number of HSDs, contributing to the 1950-1960s increase. The 1951 and 1953 seasons had anomalously warm winter seasons, whereas the 1959, 1962, 1963, 1965, and 1967 seasons were anomalously cold. The 1954 season is interesting, as there were varied anomalies and only a small region of strong cold temperatures in northern Kansas. Overall, these specific seasons led to the 1950s and 1960s experiencing the greatest number of extreme temperature swings.

Interestingly, in the latter half of the time series there was a decrease in extreme HSD frequency through the 2010s. However, in the 2020s there have already been 4 extreme HSDs. Comparing this to Figure 3.3, we find that HSDs did not just increase in this decade, but their extremes did as well.

With increasing extreme HSDs since the 1990s, their TSI magnitude can suggest how rapid and drastic of a temperature swing is occurring. Figure 3.4b indicates a peak in magnitude in the 2000s and 2010s, with over 1 degree increase in magnitude between the 1990s and 2010s. However, there has been a decrease in TSI magnitude for extreme HSDs in the 2020s. It is possible that the 2000s' and 2010s' increases are a result of the limited sample size, having only 2 extreme HSDs each (the 2020s have double the frequency of the 2010s).

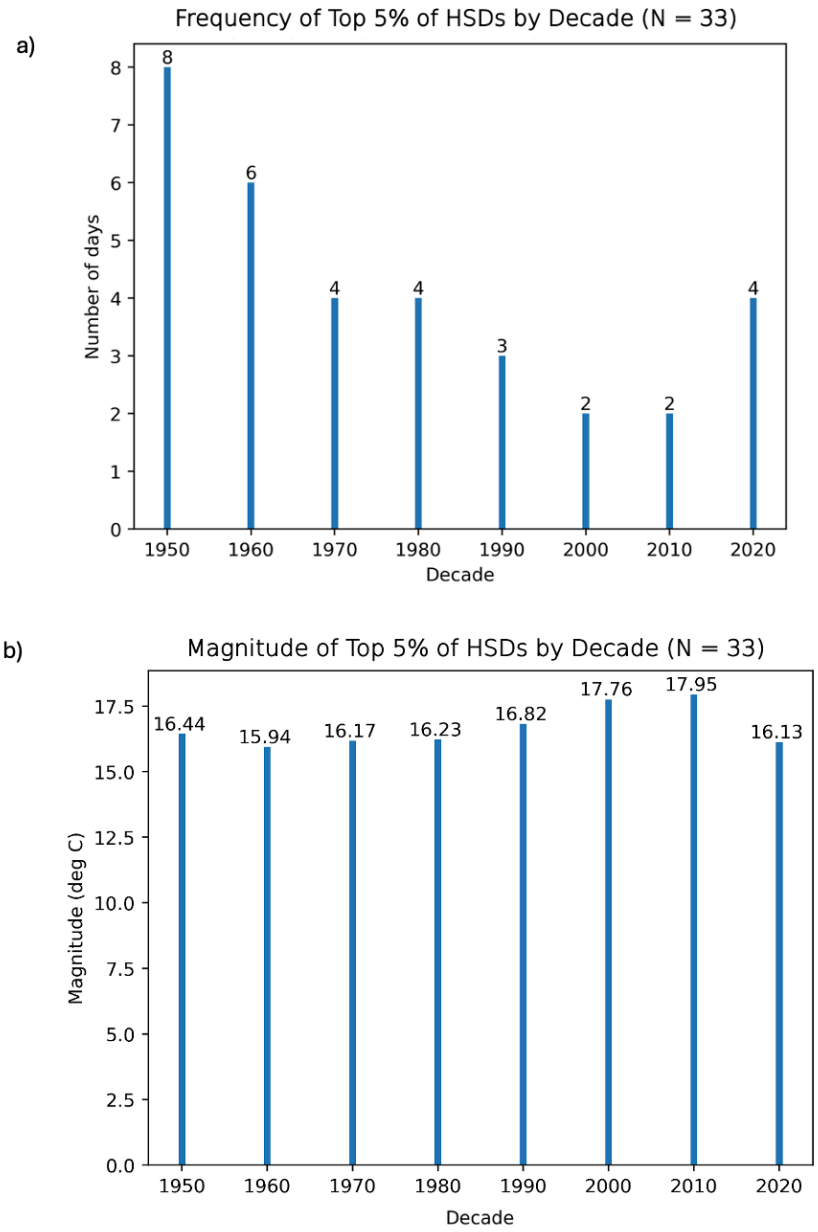

Figure 3.4: (a) Average frequency (days) and (b) average magnitude (°C) of the Top 5% of HSDs by Decade (N = 33).

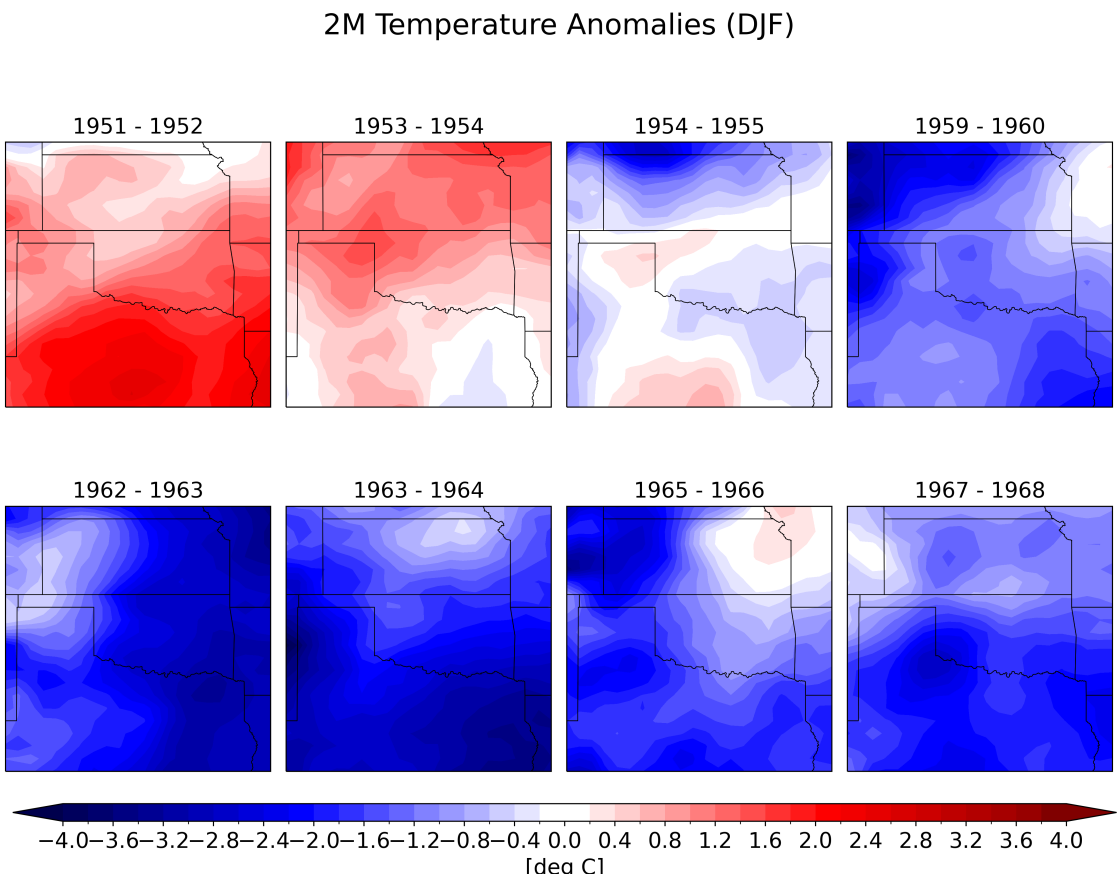

Figure 3.5: 2-m temperature anomalies (°C) for winter seasons in the 1950s and 1960s with greater than 9 HSDs.

3.2 Trends in Southern Plains Temperature Whiplash Events

Average magnitude and frequency trends can also be considered for the two types of temperature whiplashes, adding additional relevance to whether the increased frequency of HSDs is translating into an increased number of whiplash events. By design

the temperature anomalies for the 4 days prior to and following the HSD for the hot-to-cold whiplashes are positive and negative respectively, and vice versa for the cold-to-hot whiplash events (Figure 3.6). The hot-to-cold whiplash anomalies (Figure 3.6a) have a stronger average whiplash slope magnitude from day -1 to day 1 (about -5.79 °C/day) than the cold-to-hot whiplash anomalies (about 4.83 °C/day; Figure 3.6b). Hot-to-cold whiplashes also reach a greater average temperature anomaly magnitude on lag day 1. Finally, while the criteria only requires the temperature anomalies to be negative for 4 days before the HSD, all of the cold-to-hot whiplashes remained anomalously cold up to 6 days prior to the HSD. This suggests that the cold anomalies tend to persist longer than the warm anomalies in the winter. This could be due to multiple reasons, including blocking patterns that allow Arctic air into the mid-latitudes (Loikith and Broccoli 2012; Westby and Black 2015; Xie et al. 2017), warm Arctic conditions, or a weaker polar jet stream (Cohen 2016; Francis and Vavrus 2012). Additionally, the distribution of 2-m temperature anomalies over the Southern Plains in the wintertime is left-skewed, meaning in general there are more anomalously cold temperatures over the domain in the winter (Figure 3.7). Next, we will break down the specific whiplash types to analyze their frequency and magnitude trends.

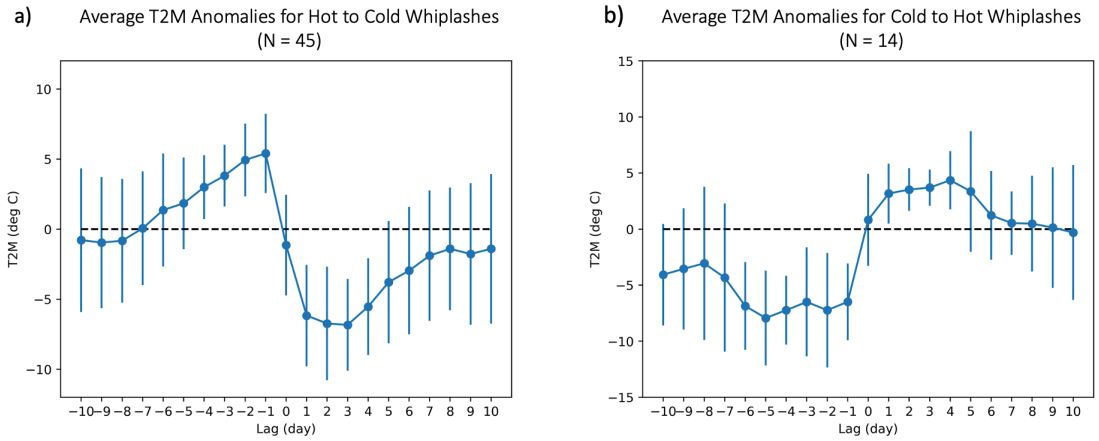

Figure 3.6: Averaged daily lagged 2-m temperature anomalies for (a) hot-to-cold and (b) cold-to-hot Whiplashes (°C). Error bars represent one standard deviation.

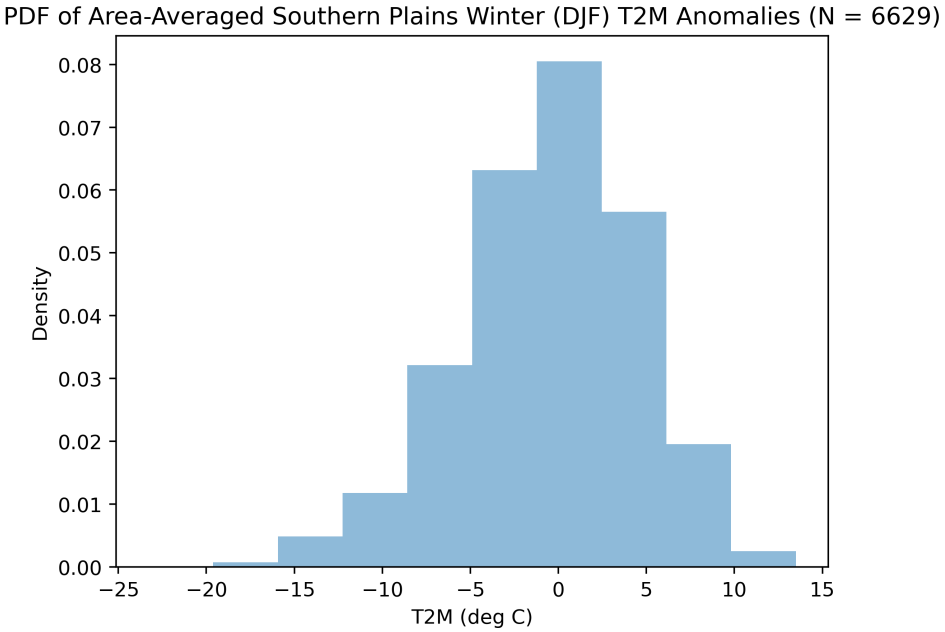

Figure 3.7: Area-averaged daily 2-m temperature anomalies (°C) over the Southern Plains domain in the wintertime from 1950-2023 (DJF; N = 6629).

3.2.1 Hot-to-Cold Whiplashes

Figure 3.8 illustrates the number of whiplash events each season categorized as hot-to-cold whiplashes. 33 of the 73 winter seasons had a hot-to-cold whiplashes occur, and 11 winters had 2 or more events. Additionally, 24 of the hot-to-cold whiplashes occurred in the earlier half of the time series (1950-1985), and 21 hot-to-cold whiplashes occurred in the latter half.

Figure 3.9 displays consistency in the number of hot-to-cold whiplashes per decade in the earlier part of the record, with 7 each in the 1950s, 1960s, and 1970s. However, following those decades, there has been considerable variability. The 1980s had the lowest recorded number of whiplashes with only 4, closely followed by the 2000s with 5. The 2010s surpassed the previous decades, with 9 occurring. Interestingly, there has not been any hot-to-cold whiplashes in the 2020s so far.

The average TSI magnitudes for hot-to-cold whiplash events also exhibit variability (Figure 3.10). From the 1950s-1970s, the TSI magnitude was greater than 10.5°C, however declined to an average below 10°C in the 1980s and 1990s. The last two decades experienced a return to these higher magnitudes, with magnitudes of 10.76°C and 10.38°C respectively. While it was not specifically examined in this study, the drop in magnitude in the 1980s and 1990s could be a result of teleconnection patterns. For example, the 1980s and 1990s had an increased number of El Niño episodes, which may have reduced the temperature variability during these decades (Christy et al. 2001). This is supported by a lower average daily TSI during these decades, as shown in Figure 3.11. Therefore, our results suggest the number of hot-to-cold whiplashes has varied since the 1980s, with an uptick in hot-to-cold whiplashes in the 2010s, and the magnitude of these whiplashes has been variable over the time record.

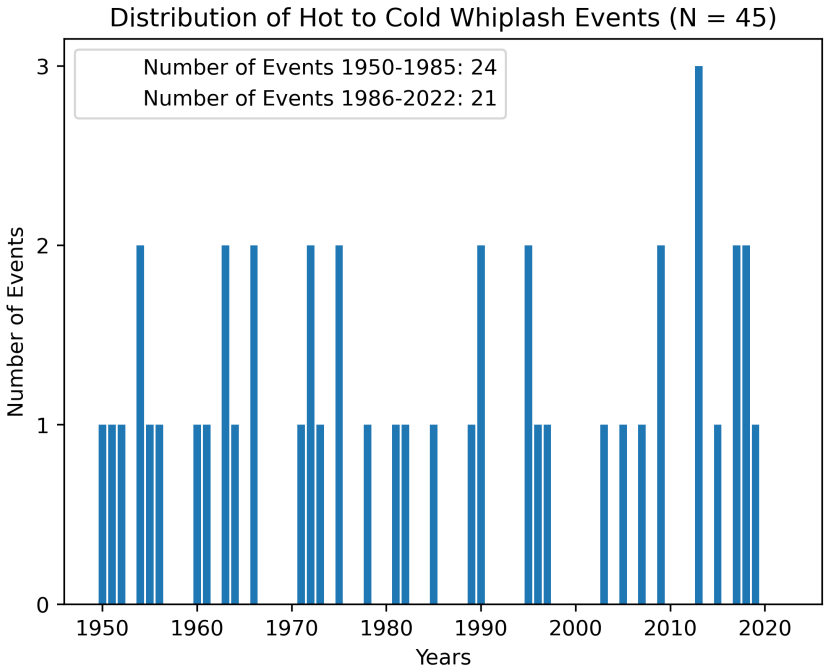

Figure 3.8: Average frequency (number of events) of hot-to-cold whiplashes by year (N = 45). The box states the number of these events that occurred in the earlier vs latter half of the time series.

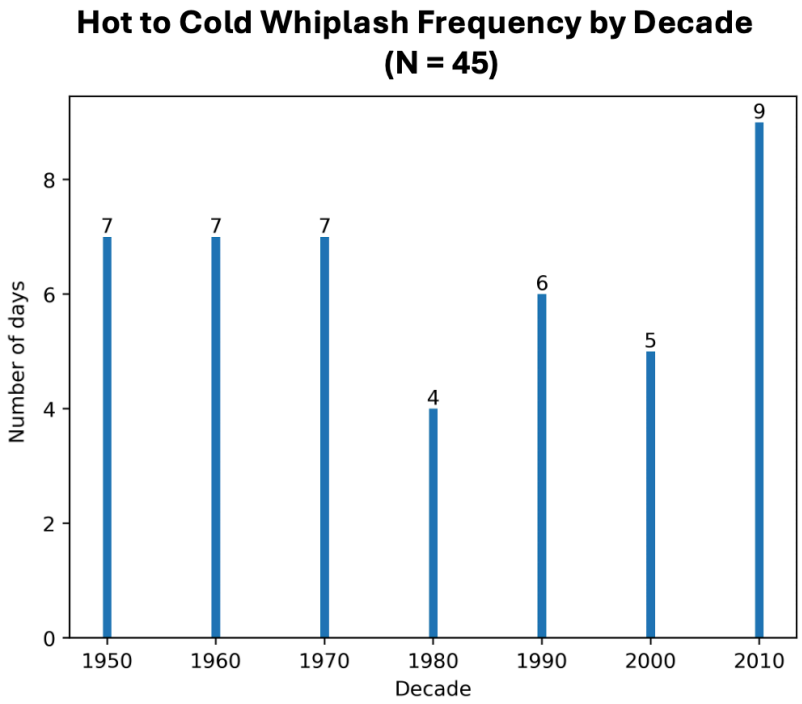

Figure 3.9: Average frequency (days) of hot-to-cold whiplashes by decade (N - 45).

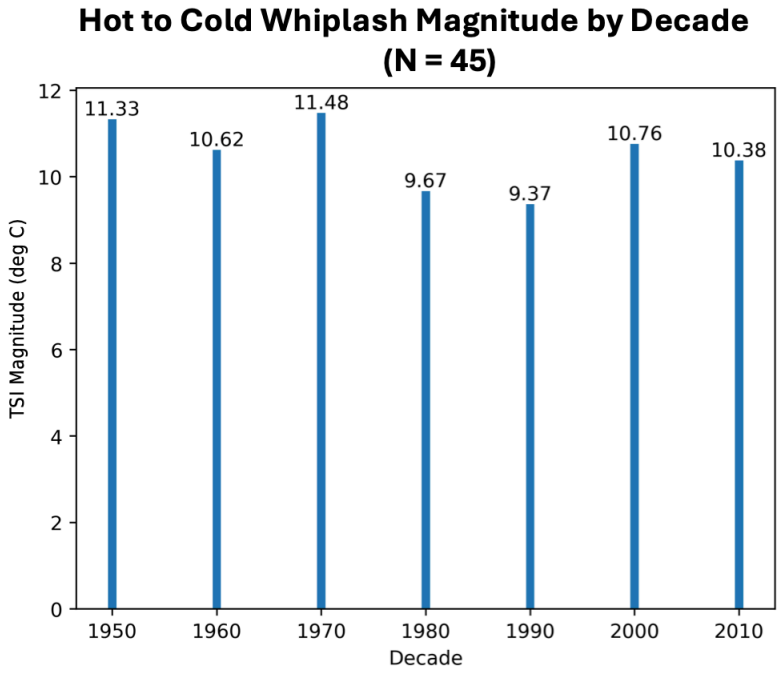

Figure 3.10: Average magnitude (°C) of hot-to-cold whiplashes by decade (N = 45).

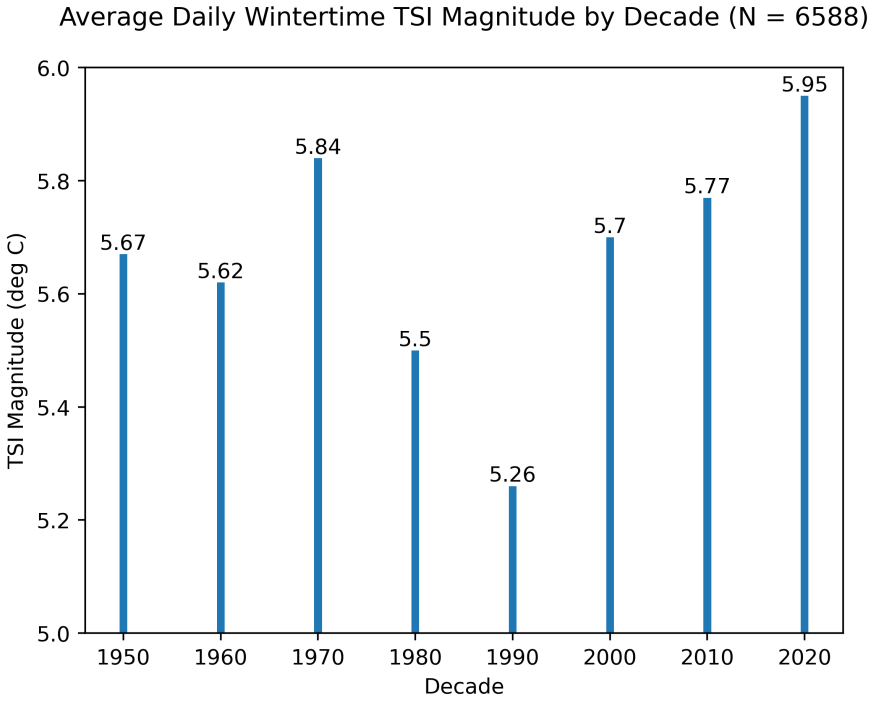

Figure 3.11: Average magnitude (°C) of the daily wintertime TSI by decade (N = 6588).

3.2.2 Cold-to-Hot Whiplashes

For cold-to-hot whiplashes, the limited sample size makes it challenging to make firm conclusions. Figure 3.12 indicates only 13 of the 73 winter seasons in the period had a cold-to-hot whiplash occur. Of these, only 1979 had 2 occur in the same year. The first half of the time series contained 6 of these events while the latter half had 8. There has also been no increase in the number of events by decade, with the last 3 decades only having one cold-to-hot whiplash each.

Looking at cold-to-hot whiplashes by decade provides better insight into their trends. Figure 3.13 indicates a peak in cold-to-hot whiplashes in the 1970s with 4 occurring, while the 1980s and 1990s only have one less each. The 1970s experienced 11 total (hot-to-cold and cold-to-hot) whiplashes, with one year (1975) having one of each (Figures 3.8 and 3.12). The 1970s featured an increase in the amount of cold days over the US Southern Plains, which may have led to more persistent cold anomalies, and therefore the potential for more whiplashes (Higgins et al. 2022; see their Figure 6). Examining the TSI magnitude of cold-to-hot whiplashes, Figure 3.14 indicates no consistent trend of average TSI magnitude. Note that the 1960s had no cold-to-hot whiplashes. Additionally, the 1990s had a lower swing magnitude for both the cold-to-hot and hot-to-cold whiplashes. While there has been a slight peak in TSI magnitude over the 2010s and 2020s, this is not a large change from the 1970s and 1980s.

In summary, the frequency of HSDs and hot-to-cold whiplashes have increased over the last 1-2 decades. The most extreme HSDs have increased throughout the most recent decade despite only 11 winter months so far. Cold-to-hot whiplashes have decreased, with only 1 cold-to-hot whiplash per decade since the 2000s. However, cold-to-hot whiplash magnitude is variable, with a decline in the 1990s and 2000s. To

determine what may be leading to these changing trends, the atmospheric patterns of the whiplash types will be explored in the next chapter.

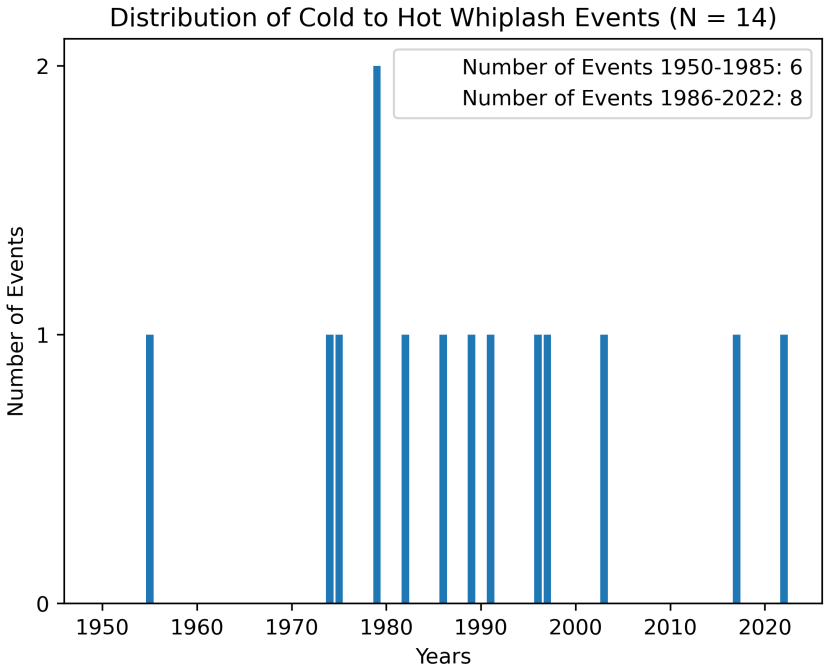

Figure 3.12: Average frequency of cold-to-hot whiplashes by year (N = 14). The box states the number of these events that occurred in the earlier vs later half of the time series.

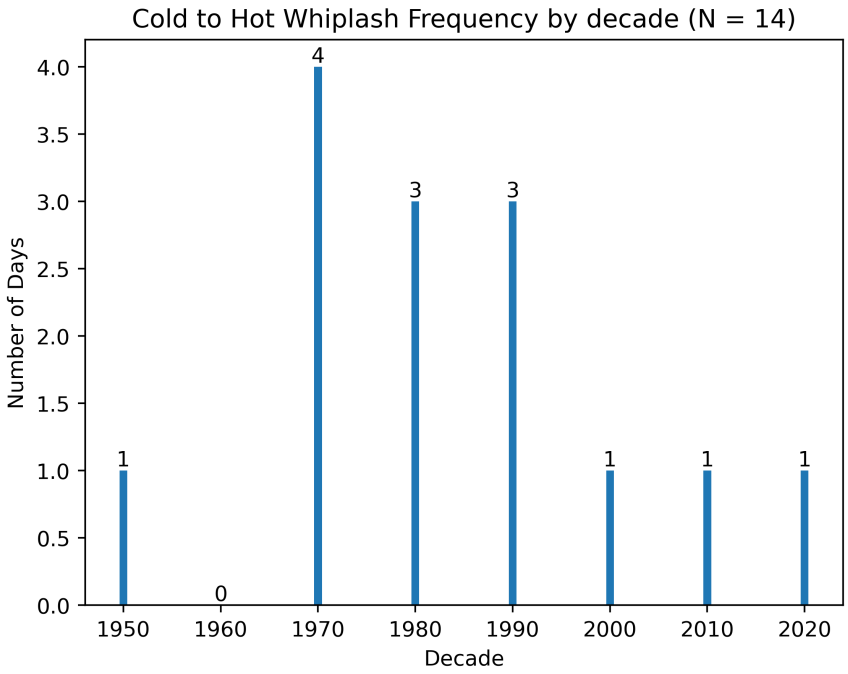

Figure 3.13: Average frequency (number of events) of cold-to-hot whiplashes by decade (N = 14).

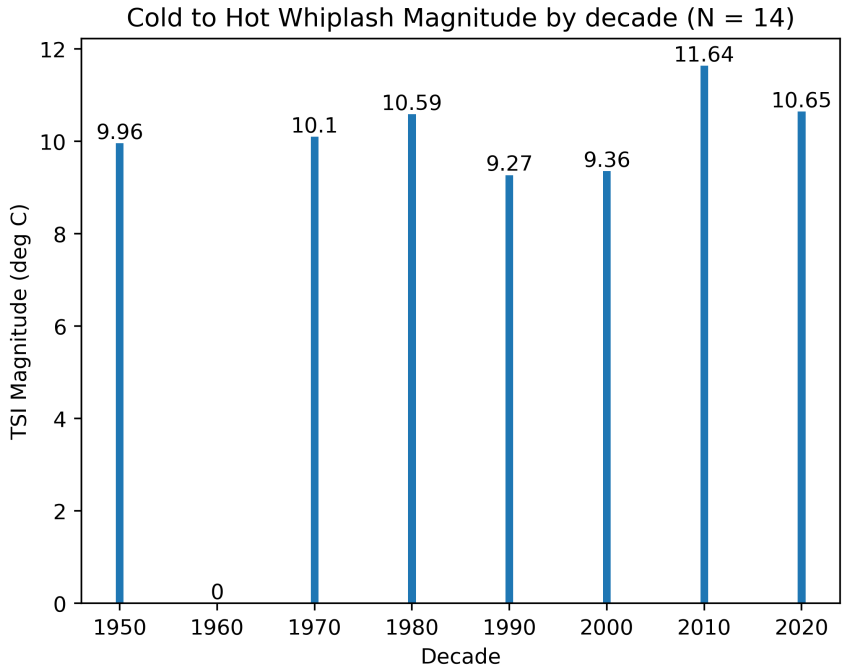

Figure 3.14: Average Magnitude (°C) of cold-to-hot whiplashes by decade (N = 14).

Chapter 4

Evolution and Characteristics of Temperature Whiplashes

Through investigating the evolution of the atmospheric flow, we can determine what precursors in the atmospheric circulation are present and eventually lead to temperature whiplashes. The precursors examined in this chapter are specifically useful for prediction in the S2S range, and while beyond the context of this thesis, could potentially be utilized in modeling experiments to predict future temperature whiplashes, as they persist prior to and during the whiplashes and can be identified in advance of the event.Our analyses include both tropospheric and stratospheric phenomena, as well as their subsequent interactions. We will present precursors for both types of whiplashes, and close with a comparison of their characteristics.

4.1 Hot-to-Cold Whiplashes

4.1.1 Mid-Tropospheric Flow during Hot-to-Cold Whiplashes

To examine the mid-level tropospheric flow associated with hot-to-cold whiplash events in the US Southern Plains, we began by compositing the 500-hPa geopotential heights and anomalies. Figure 4.1 presents composites of the lagged 500-hPa geopotential height anomalies for hot-to-cold whiplashes over 3-day periods. Lag day 0 is the corresponding HSD. From days -5 to -3 there is relatively zonal flow across the US Southern

Plains, however there is anomalous ridging over the north Pacific, anomalous troughing over Alaska and northwestern Canada, anomalous ridging over the north Atlantic, and positive height anomalies over most of the US (Figure 4.1a). The positive height anomalies over the US align with the anomalously warm period in the hot-to-cold whiplash. As the pattern progresses, the ridging feature in the north Pacific intensifies and moves eastward over Alaska (Figure 4.1b). This Alaskan Ridge creates a significant blocking pattern and amplifies the downstream flow. The trough that was originally over Alaska deepens over the western US and moves across the Southern Plains between days 1-3 (Figure 4.1c). Positive 500-hPa geopotential height anomalies over the eastern US exist prior to the HSD, but propagate into the Atlantic Ocean following the HSD. Subsequently, the trough over the US becomes more progressive again. However, while it weakens by days 4 to 6, the Alaskan Ridge remains strong and present for at least 6 days following the HSD (Figure 4.1d). In summary, the persistent blocking pattern in the troposphere is associated with the persistent cold anomalies present in the hot-to-cold whiplashes. To determine what may be leading to this blocking pattern, we can consider possible interactions with the stratosphere.

4.1.2 Interactions with the Stratosphere leading to Blocking

As previously mentioned, variability of the SPV is greatest in the winter months and can have a substantial impact on tropospheric temperatures (Baldwin and Dunkerton 2001; Thompson and Wallace 2000; Lee et al. 2019). To examine the SPV mean characteristics, we chose the 50-hPa and 10-hPa pressure levels. At 50-hPa, there are 2 clear areas of anomalies -5 to -3 days before the HSD (Figure 4.2a). There are negative anomalies over the Beaufort Sea and Siberia, and positive anomalies over the north Atlantic Ocean and northeastern Russia. As the HSD approaches, the anomalies

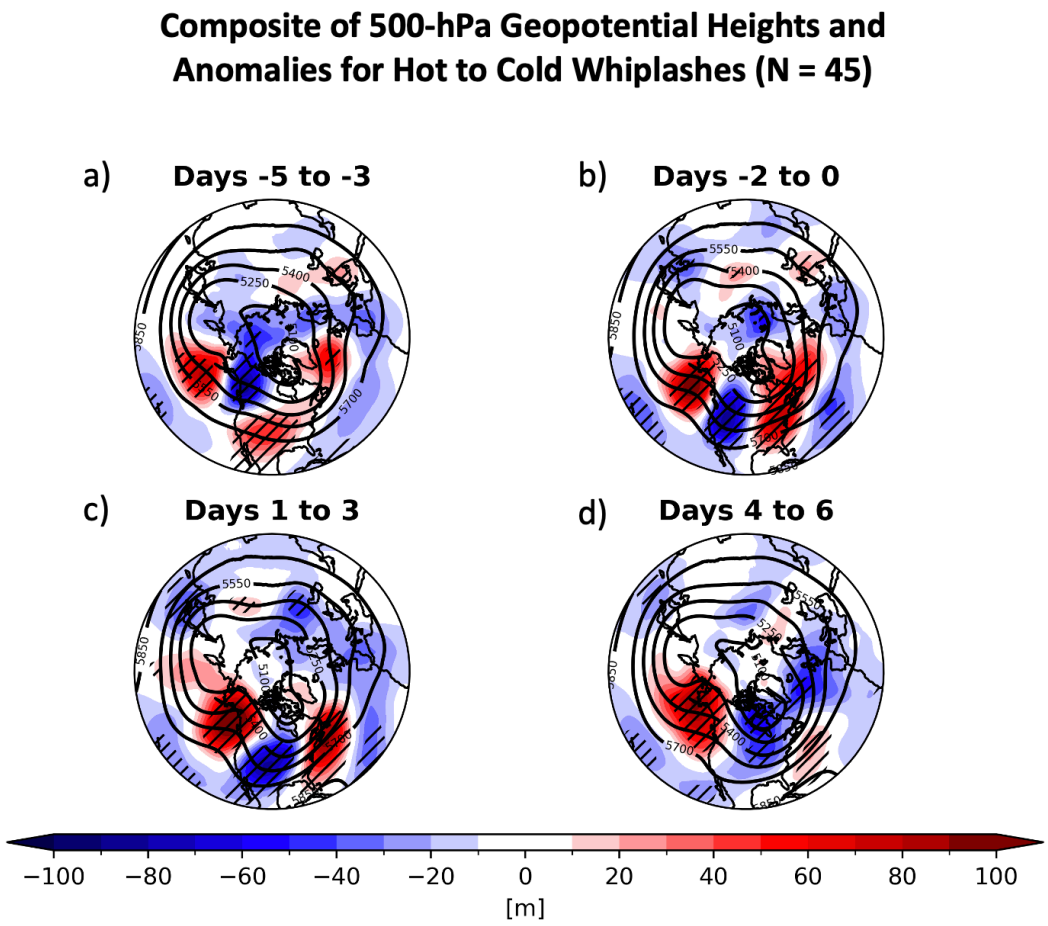

Figure 4.1: Lagged 500-hPa geopotential heights (meters; contours with a contour interval of 150m) and anomalies (meters; shading) for hot-to-cold whiplashes over lagged (a) days -5 to -3, (b) days -2 to 0 , (c) days 1 to 3, and (d) days 4 to 6 (N = 45). Hatching represents where anomalies are significant at the $p < 0.05$ level.

weaken slightly, but extend into Canada and the Northern US (Figure 4.2b). By the HSD and during the 3 days that follow, there are 2 areas of statistically significant anomalies, associated with stretching of the SPV (Figure 4.2b-c). This stretching is evident by the height contours becoming elongated southward and becoming more meridionally-oriented. Finally, days 4-6 there is a strong negative anomaly amplifying over the Canadian Archipelago (Figure 4.2d). Furthermore, in the upper stratosphere at 10-hPa (Figure 4.3), there are statistically significant positive anomalies over the US Southern Plains prior to the HSD, but following the HSD they are exclusively in Asia.

Most of the high latitudes feature higher than average heights, indicating a warmer, weaker SPV. A possible reason for SPV stretching is wave reflection, which occurs when tropospheric waves propagate in the vertical and reflect off of the SPV (Perlwitz and Harnik 2003; Kodera et al. 2008; Harnik 2009). These impacts have downstream effects on temperature patterns, and can lead to CAOs in the United States (Lee et al. 2019; Ding et al. 2023; Millin et al. 2022).

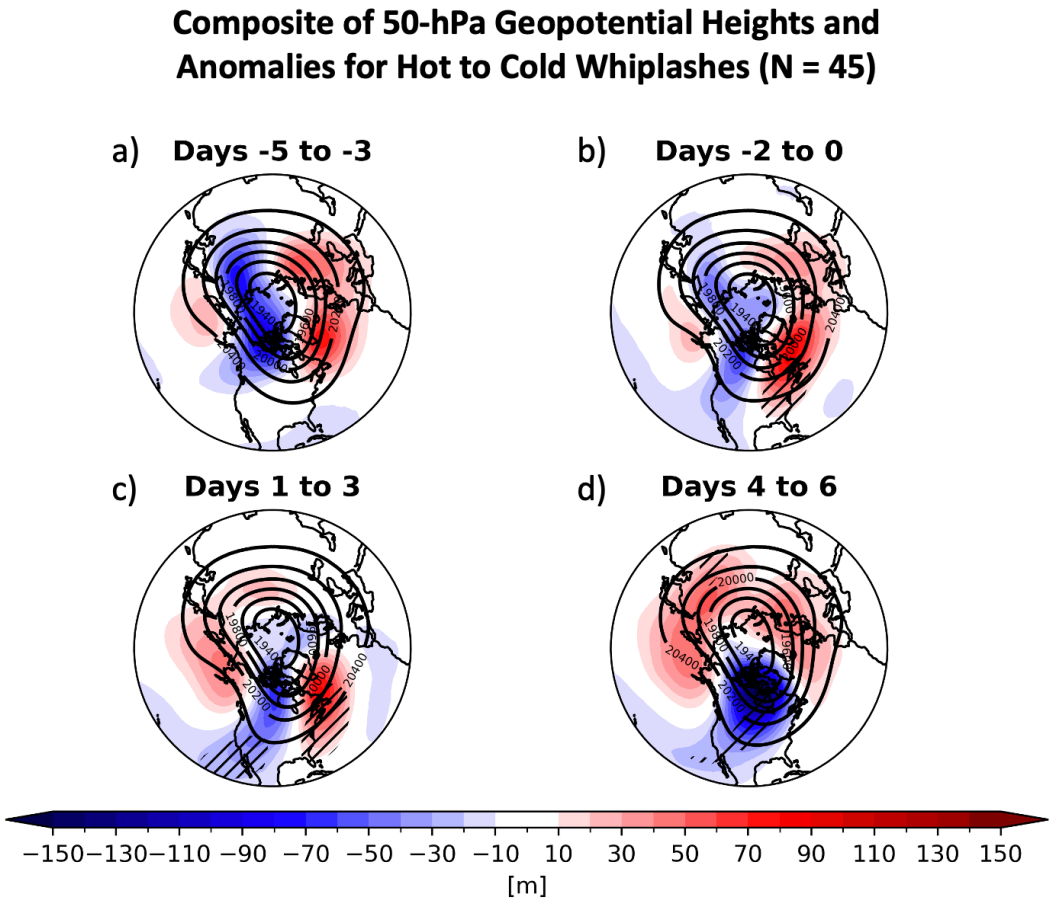

Figure 4.2: As in Fig. 4.1 but for 50-hPa geopotential heights and anomalies. Contour interval every 150m.

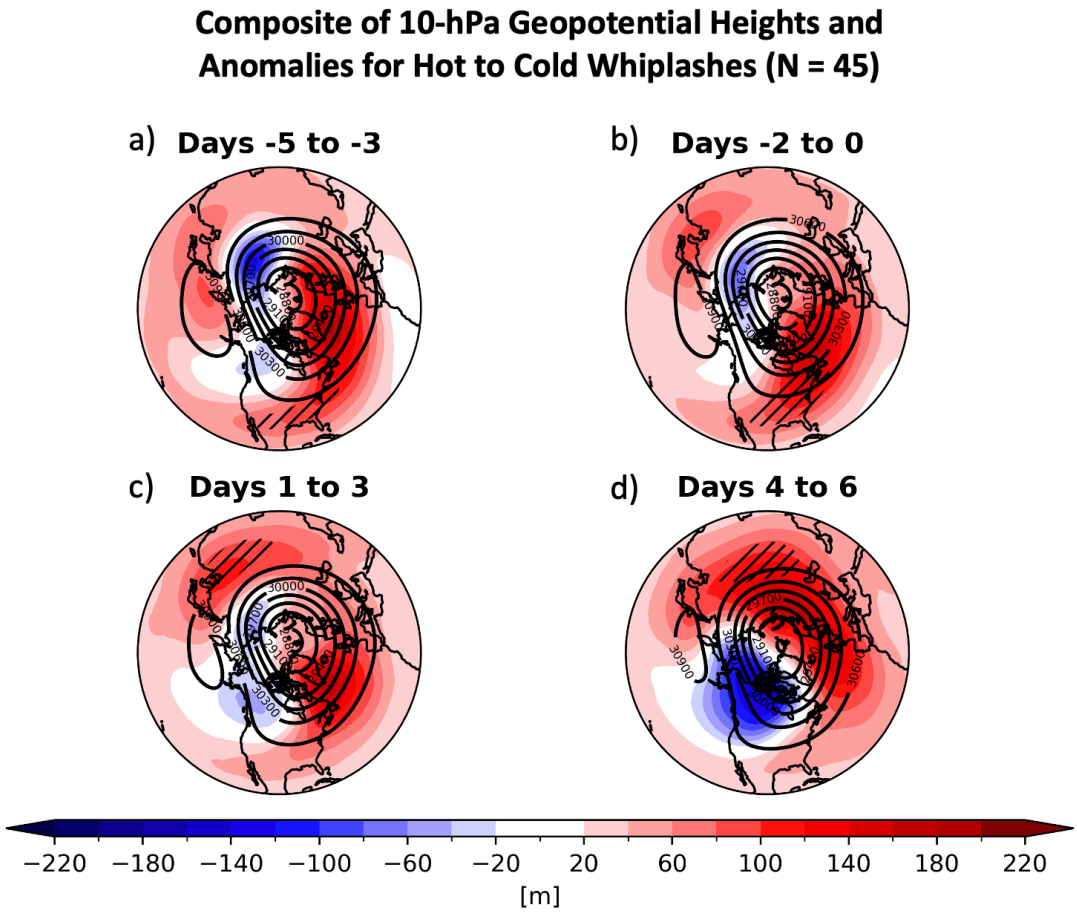

Figure 4.3: As in Fig. 4.1 but for 10-hPa geopotential heights and anomalies. Contour interval every 150m.

4.1.3 Wave Activity Flux and the Reflection Index

To determine if SPV stretching was due to vertical Rossby wave propagation and subsequent reflection into the stratosphere, we investigated the lagged 100-hPa WAFz anomalies prior to the HSD (Figure 4.4). From days -5 to -3, there is a positive, statistically significant WAFz anomaly over Siberia and a negative statistically significant WAFz anomaly over Alaska (Figure 4.4b). This WAFz anomaly pattern suggests that Rossby waves are propagating vertically over Siberia and are returning into the troposphere over Alaska. WAFz is also proportional to $v'T'$, indicating meridional eddy

heat flux anomalies in the corresponding areas (Eq. 2.3; Plumb 1985). Using this relationship, the RI was developed to categorize wave reflection events (Matthias and Kretschmer 2020).

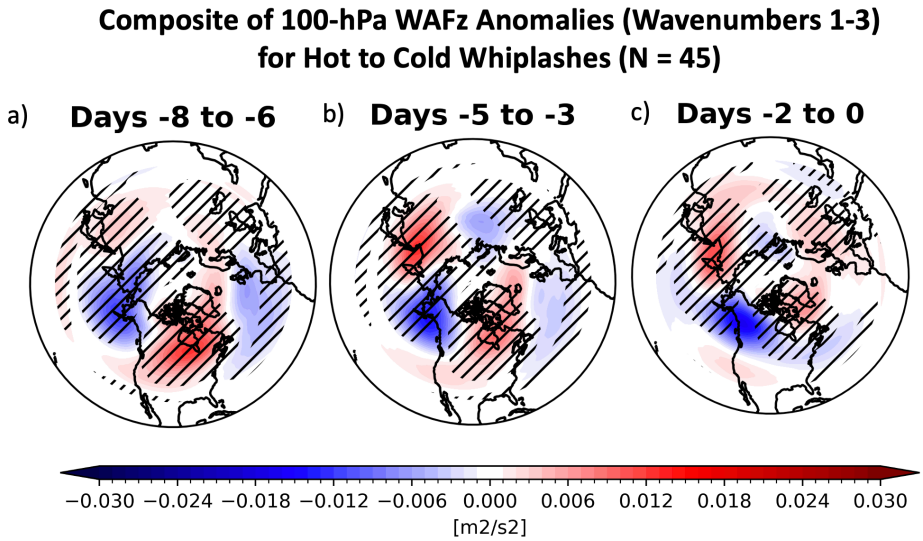

Figure 4.4: Lagged 100-hPa vertical wave activity flux anomalies (m^2/s^2; shading) in for hot-to-cold whiplashes (N = 45). Values were filtered to include only waves with wavenumbers 1-3. Hatching represents where anomalies are significant at the $p < 0.05$ level.

When the RI was calculated using the methodology from Matthias and Kretschmer (2020) (Eq. 2.5), relating to the difference in the area-averaged meridional eddy heat flux over Siberia and Canada, it did not indicate that much wave reflection was occurring (Figure 4.5). However, when we collocated the reflection regions of the RI with our events, we noticed the location of the WAFz anomalies were not being captured with the RI (Figure 4.6). The purple boxes in Figure 4.6a represent the domains used to calculate the RI. The RI domains in Matthias and Kretschmer (2020) were selected based on both a clustering of the daily 100-hpa geopotential height anomalies in Kretschmer et al. (2018) and the wave reflection case studies presented earlier in Matthias and Kretschmer (2020). The WAFz anomalies for the whiplash events are

outside of these boxes, especially the Canada box. To account for this discrepancy, we altered the reflection locations by moving the Siberia box westward, and made the Canada domain box an Alaska domain box (Figure 4.6b).

With this change, favorable reflection conditions are present prior to the HSDs (Figure 4.7). Within the -7 to -3 days window, 24 of the 45 whiplash events have a period of reflection. While this is not a feature in all of the hot-to-cold whiplash events, over half of the events represents a substantial sample size. These results suggest that the reflection domain in Matthias and Kretschmer (2020) and Messori et al. (2022) may not encompass all reflection events, a conclusion that is also echoed in Millin et al. (2022). Additionally, for our analysis we did not enforce the criterion of a 10-day reflection period due to the rapidity of these events. Matthias and Kretschmer (2020) and Messori et al. (2022) considered CAOs, which had long-duration cold anomalies, whereas whiplash events only require a cold period for 4 days. The cold period presented in this study is also defined as a negative 2-m temperature anomaly, not a period of cold below the 5th percentile, which was the case in Messori et al. (2022) and Millin et al. (2022). We did not specifically plot the wind profiles, so while we can suggest reflection using our composites and the RI, we cannot confirm this without future work. Overall, improving prediction of wave reflection could enhance prediction of whiplash events in the weather and subseasonal time frames.

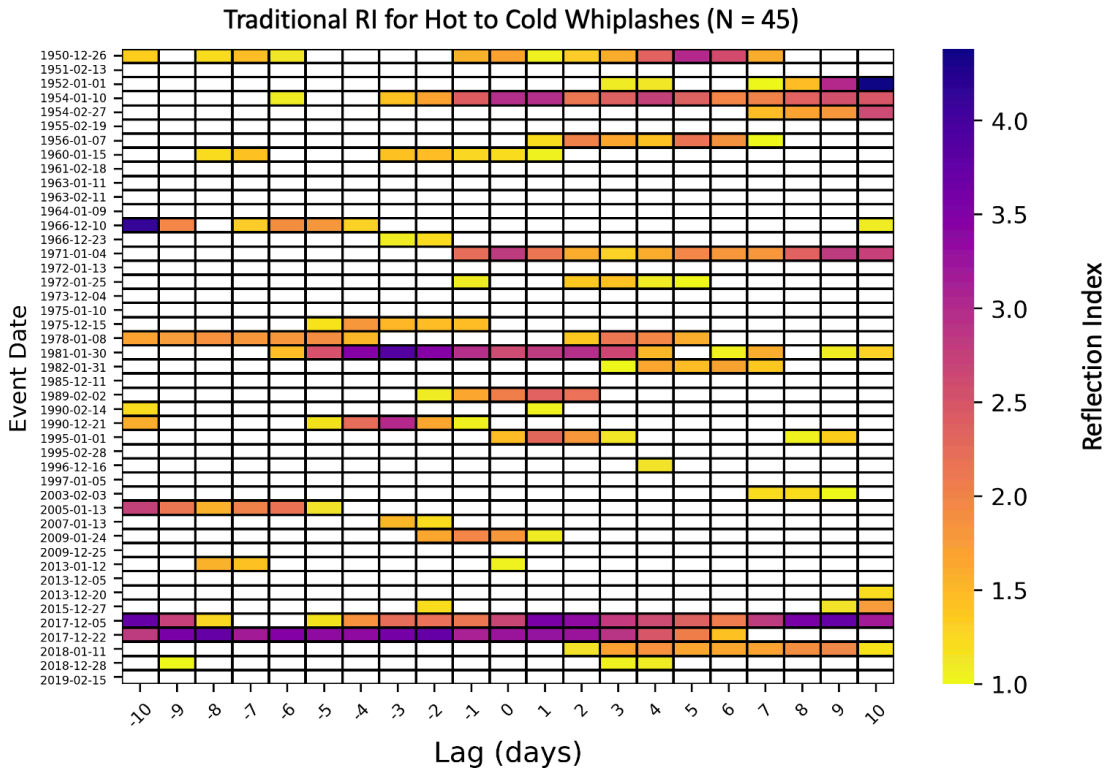

Figure 4.5: Lagged heatmap of Reflection Index values from Matthias and Kretschmer (2020) for hot-to-cold whiplash events (N = 45). Event dates are categorized by the corresponding HSD.

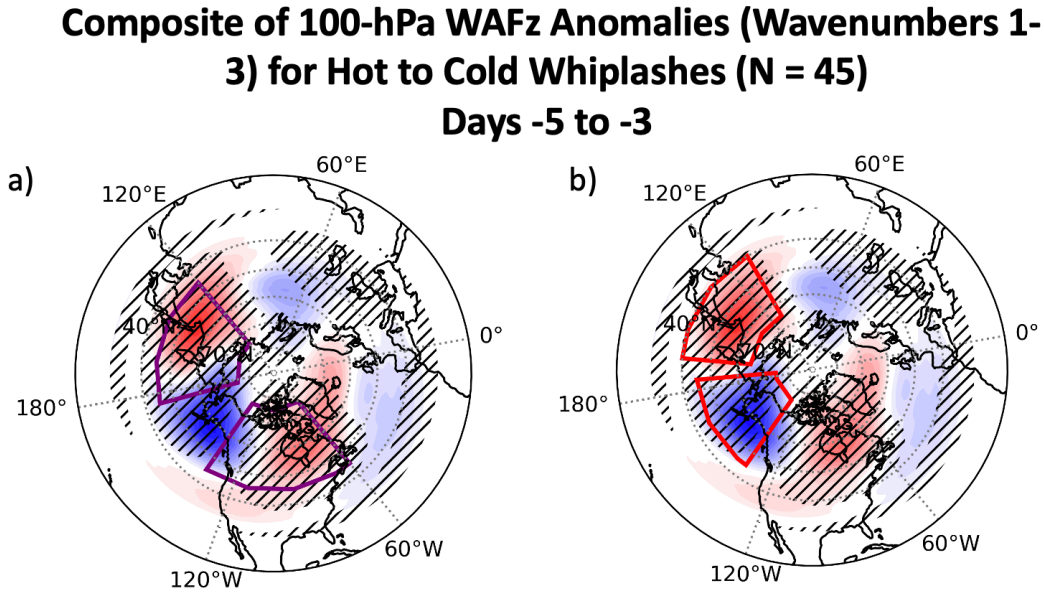

Figure 4.6: Days -5 to -3 panel from figure 4.4, with RI domains from (a) Matthias and Kretschmer (2020) (purple boxes) and (b) this study's proposed new boxes (red boxes). Hatching represents where anomalies are significant at the $p < 0.05$ level.

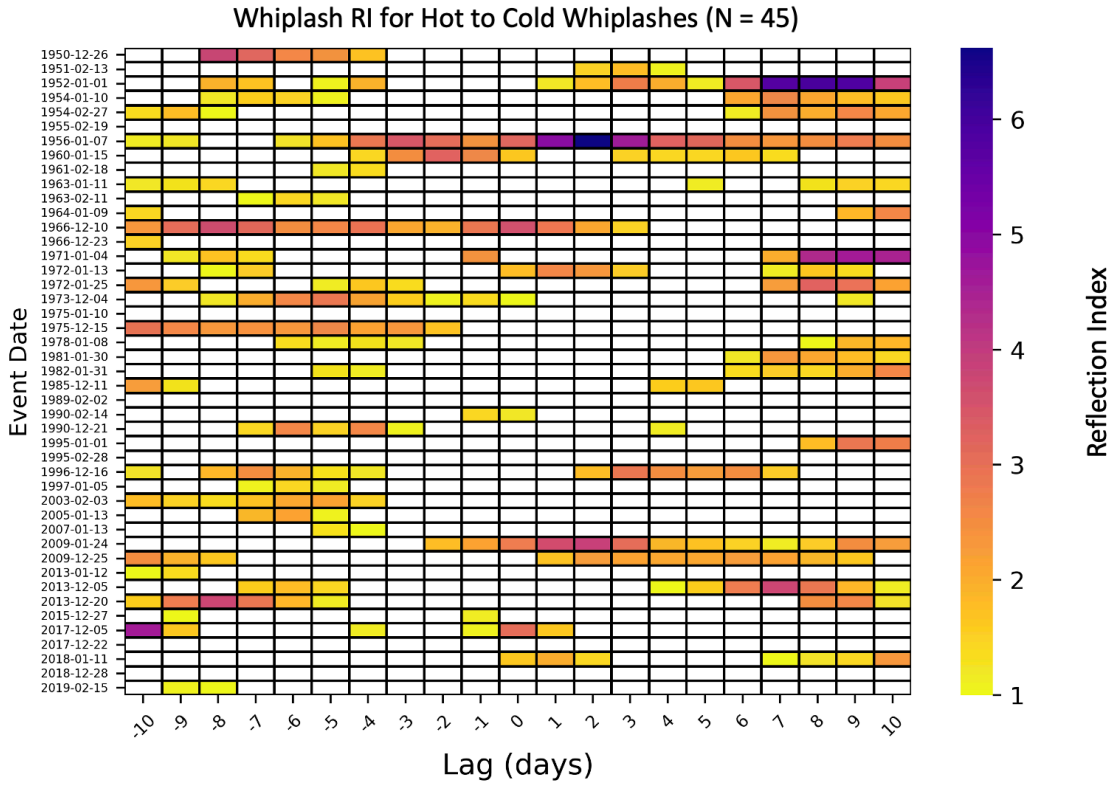

Figure 4.7: Lagged heatmap of Reflection Index values from the new Whiplash Reflection Index for hot-to-cold whiplash events (N = 45). Event dates are categorized by the corresponding HSD.

4.1.4 Weather Regimes associated with Hot-to-Cold Whiplashes

Another way to examine favorable flow patterns associated with temperature whiplash events are through weather regimes. Weather regimes are different from weather patterns, as they persist longer and can be used as a framework to categorize longer atmospheric flow patterns (Charlton-Perez et al. 2018; Lee et al. 2019; Millin et al. 2022). Certain regimes persist longer than others, and are more likely to transition to and from other regimes (Charlton-Perez et al. 2018; Lee et al. 2019). Additionally, they can be used to suggest the strength of the SPV. There are 3 dominant weather regimes for hot-to-cold whiplashes based on their HSD regime: Arctic High (ArH, 15 events), Alaskan Ridge (AkR, 14 events), and Arctic Low (ArL, 10 events; Figure 4.8). The Pacific Trough (PT) and West Coast Ridge (WCR) do not occur frequently, which aligns with the 500-hPa geopotential height composite of the hot-to-cold whiplashes, as both regimes feature anomalous troughing over Alaska. To explore the whiplash events' SPV strengths, we break down each dominant regime and examine their weather regime evolutions.

The evolution of the ArH regime (Figure 4.9) indicates at least two days of an ArH regime around the whiplash day (with exception of the 1954-02-27 event), with either lag day -1 or 1 also being in the ArH regime. Prior to day 0, 13 out of the 15 events have PT or ArH transitions within 10 days before the HSD. This is similar to the results in Millin et al. (2022), which found CAOs that occurred in an ArH regime generally have a persistent ArH regime for at least a week or longer prior to CAO onset. Ten of the events have at least 1 PT regime day in the 10 days preceding the ArH HSD, and 6 events have at least 3 consecutive PT days. In Millin et al. (2022), 8 of the 18 CAOs they identified had at least 1 day in the PT regime within the 10 days

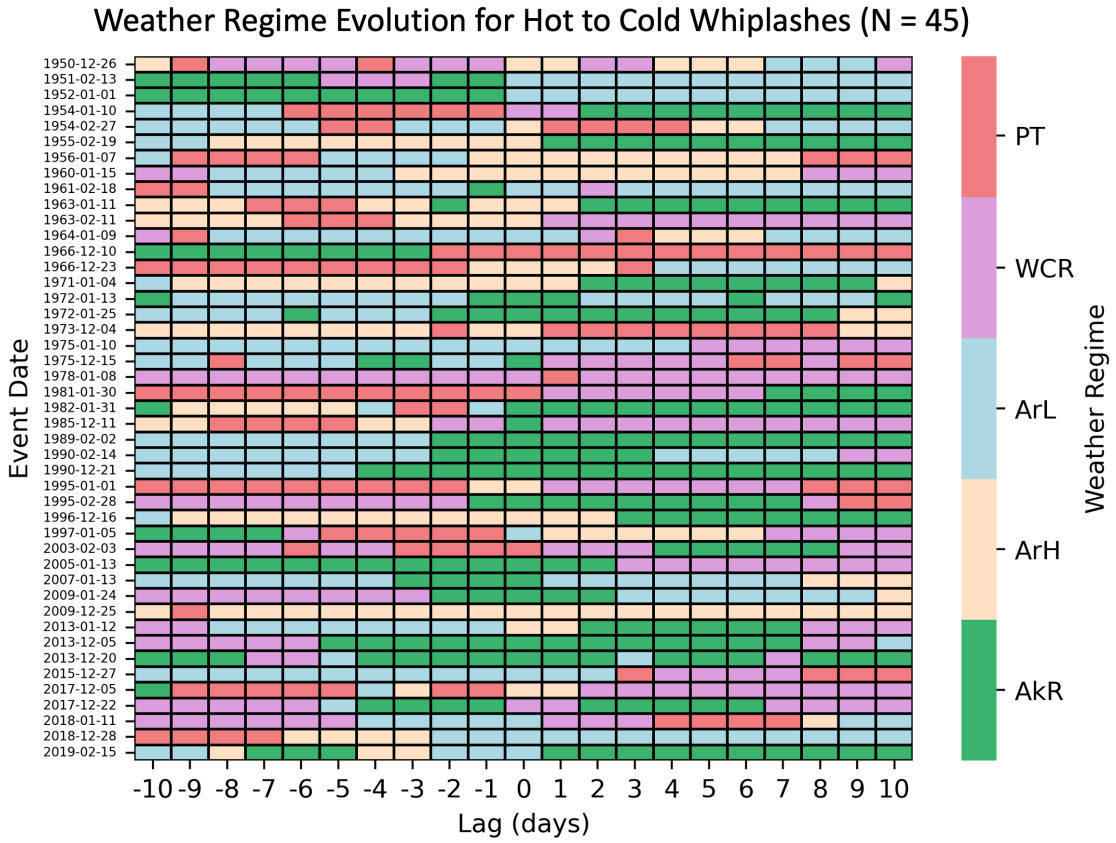

Figure 4.8: Evolution of North American winter weather regimes for hot-to-cold whiplashes (N = 45). Event date on y-axis is each event's corresponding HSD.

preceding the CAO. Since the PT regime is characterized by negative stratospheric geopotential height anomalies, the PT regime is generally associated with a stronger SPV. The opposite is true for an ArH regime, suggesting a weaker SPV (Lee et al. 2019; Millin et al. 2022). Thus, the transition from a PT to ArH regime suggests a decline in SPV strength around the HSD.

Since whiplashes are rapid swing events and do not have cold anomalies as persistent or as strong as CAOs, a long, persistent ArH regime is only observed in about 5 of the events. Four events transition from ArL to ArH 1-3 days before the HSD. This transition is supported by the 500-hPa geopotential height anomalies (Figure 4.1), which depict anomalous troughing in the day -5 to -3 range over Alaska. Depending on

how quickly the Rossby wave train moves into the blocking ridge pattern, it is possible that this regime transition occurs if the transition to the block is slower, setting up the blocking pattern closer to the HSD. The transition from an ArL to ArH regime also supports the conclusion of a transition from a strong to weak SPV.

Following the ArH HSD, there are certain patterns that the whiplash events evolve into. Contrary to the antecedent persistent ArH regime, only 3 of the events have 3 or more consecutive ArH days immediately preceding the HSD. However, 8 of the 15 events immediately transition into persistent AkR or WCR regimes. Since the blocking pattern remains even through 6 days following the HSD (Figure 4.1), both the AkR and ArH patterns have anomalous ridging over Alaska, with AkR having a more intense block. The events that transition to these regimes may be indicative of a longer blocking pattern, and possibly longer-lasting cold anomalies. In summary, the ArH regimes whiplashes are indicative of hot-to-cold whiplashes that occur in an either already weakened SPV, or the transition from a strong to weak SPV.

The second dominant regime is the AkR, which shows distinct patterns preceding and following the HSD (Figure 4.10). This regime is important as prior research has indicated that this regime led to the most intense CAOs for the US Southern Plains (Lee et al. 2019; Millin et al. 2022). In general, 11 of the 14 events transitioned to the AkR regime prior to the HSD, with all but 2 events (the 1982-01-31 and 1985-12-11 events) transitioning from an ArL or WCR regime. The ArL regime is generally linked with a stronger SPV, and suggests whiplash transitions associated with anomalously strong SPVs (Lee et al. 2019; Millin et al. 2022). The WCR and AkR regimes exhibit a similar ridging pattern, with WCR being more meridionally-oriented, and therefore WCR is also a reasonable transition into an AkR regime (Lee et al. 2019; Millin et al. 2022). Following the HSD, the same regimes dominate. About 5-6 of the events remain

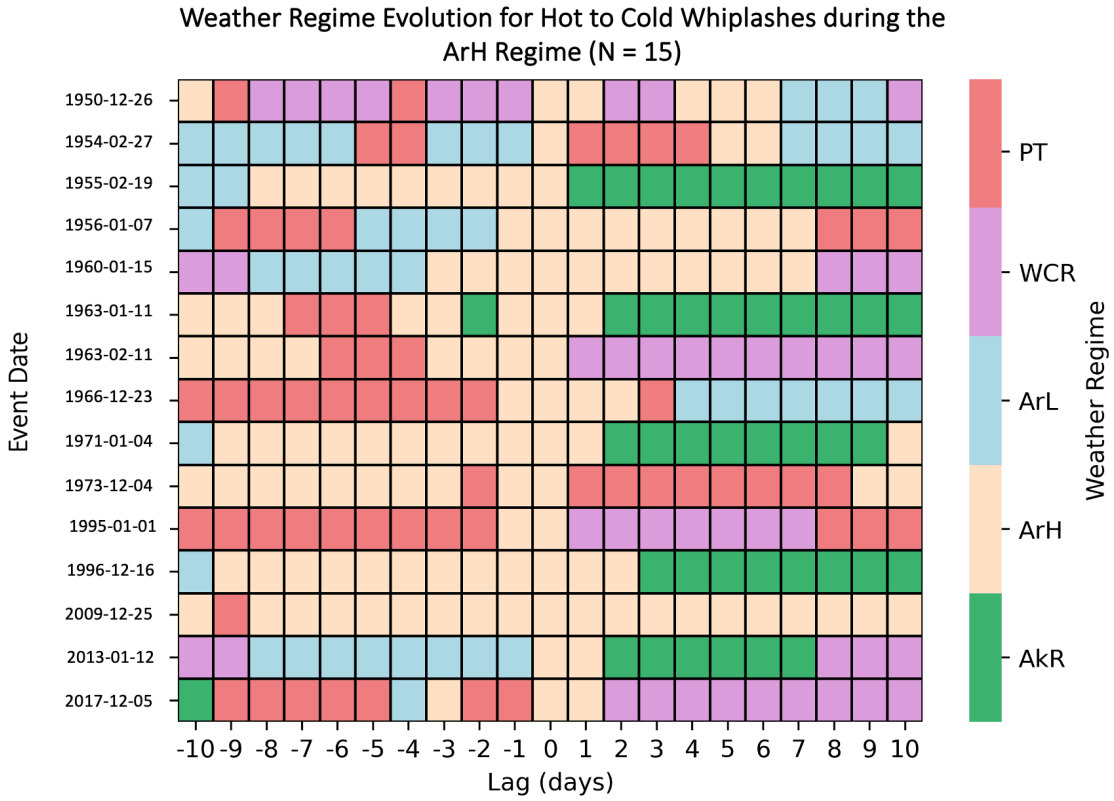

Figure 4.9: Evolution of North American winter weather regimes for hot-to-cold whiplashes with their HSD occurring during the Arctic High regime (N = 15). Event date on y-axis is each event's corresponding HSD.

in a sustained AkR regime, while about 3 transition to a WCR regime, and about 4 to an ArL regime. These transitions suggest that hot-to-cold whiplash events in the AkR regime are generally correlated with a stronger SPV. Additionally, wave reflection has been shown to occur prior to and during the AkR regime, supporting the hypothesis that wave reflection may be occurring in a subset of the hot-to-cold whiplash events (Millin et al. 2022).

The last regime to consider is the ArL regime (Figure 4.11. The ArL regime, while it has 4 and 5 events less than the AkR and ArH regimes respectively, still encompasses a large sample size when compared to the WCR and PT. Hot-to-cold

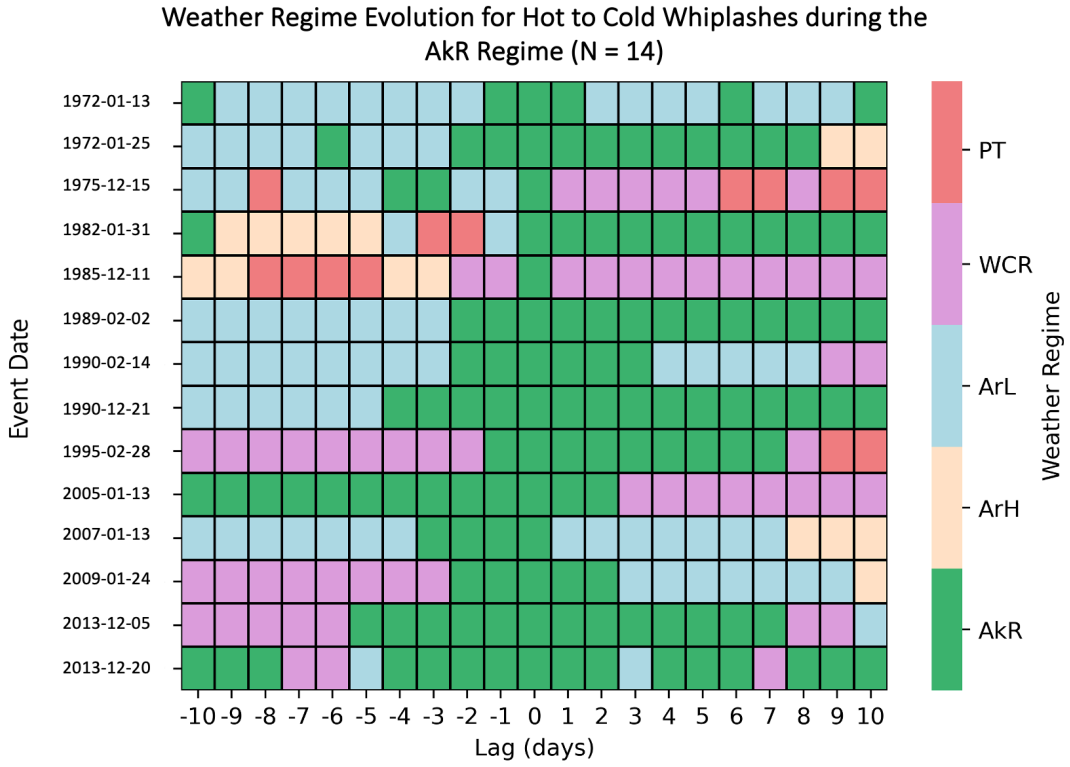

Figure 4.10: Evolution of North American winter weather regimes for hot-to-cold whiplashes with their HSD occurring during the Alaskan Ridge regime (N = 14). Event date on y-axis is each event's corresponding HSD.

whiplashes being in an ArL phase on the HSD is surprising, as an ArL pattern exhibits troughing over Alaska, whereas the 500-hPa geopotential height anomalies in Figure 4.1 illustrate ridging over Alaska. The high sample size of ArL whiplashes may be an artifact of the hot-to-cold whiplash precursors not falling into a specific regime. The most intense positive geopotential height anomalies in Figure 4.1 occur south of Alaska, as well as indicates positive geopotential height anomalies along the US East Coast, aligning with the locations in the ArL regime. While the trough over Alaska does not align with our whiplash composite, more prominent East Coast ridging as well as the blocking ridge being located further south may explain why these days are

being categorized as an ArL. The ArL antecedent regimes are not as obvious as in the AkR regime. Approximately 5 of the events are in a prolonged pattern of ArL prior to the HSD, with the other 5 events transitioning from an AkR regime (2 events), PT regime (2 events), or ArH regime (1 event). With the exception of 1 transitioning from an ArH regime, which is representative of a weaker SPV, the regimes before the HSD are generally characteristic of a stronger SPV pattern.

Overall, there are 3 weather regimes that dominate hot-to-cold whiplashes: ArH, AkR, and ArL. ArH regimes are genuinely characterized by weak SPV environments, or the transition from a strong to weak SPV environment. ArH hot-to-cold whiplashes are usually proceeded by persistent WCR or AkR regimes as well. The AkR hot-to-cold whiplashes are more common when there is a stronger SPV present, and remain in a relatively strong SPV during and following the whiplash. Lastly, ArL regimes suggest a stronger SPV, but may be more common when the blocking ridge near Alaska is farther south, or the downstream ridge over the US East Coast is enhanced. These precursors offer promise in S2S prediction of hot-to-cold whiplash events. The next section will examine the the characteristics of cold-to-hot whiplashes to determine if they have the same precursors.

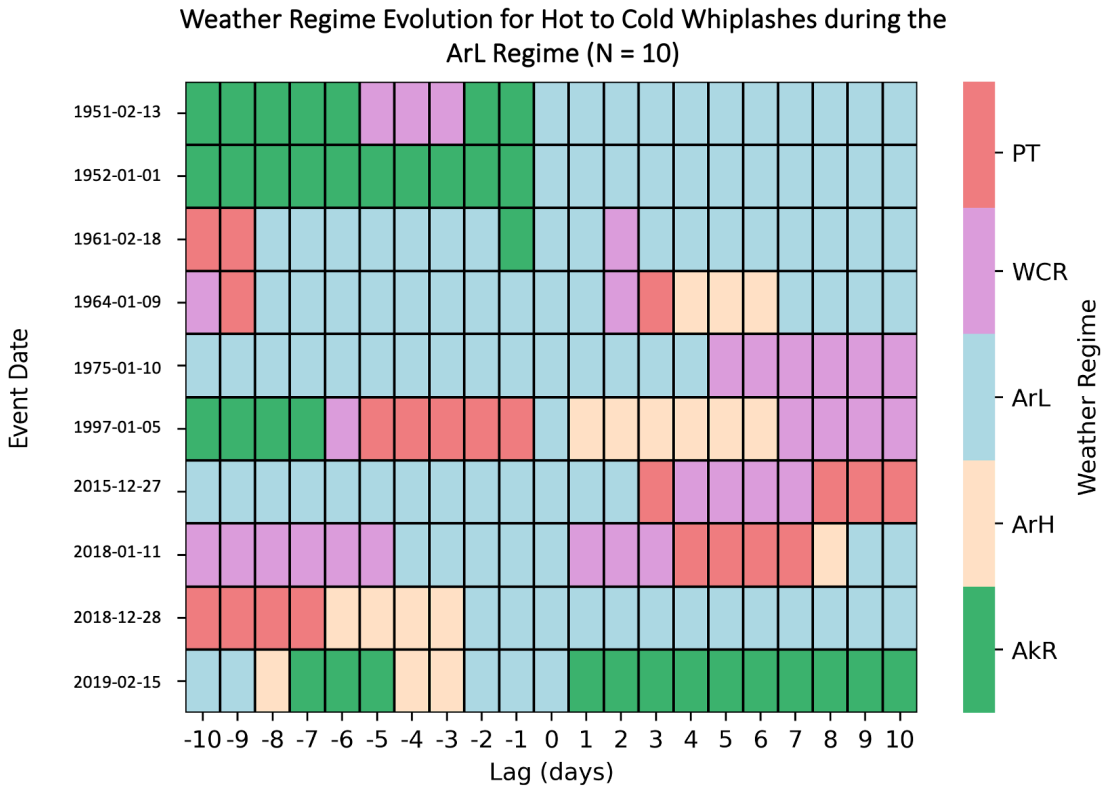

Figure 4.11: Evolution of North American winter weather regimes for hot-to-cold whiplashes with their HSD occurring during the Arctic Low regime (N = 10). Event date on y-axis is each event's corresponding HSD.

4.2 Cold-to-Hot Whiplashes

4.2.1 Mid-level Atmospheric Flow for Cold-to-Hot Whiplashes

Similar to our analysis of hot-to-cold whiplashes, we began by examining the tropospheric flow. As before, we used composite 500-hPa geopotential heights and anomalies. While a ridge exists over Alaska during days -5 to -3, the ridge is located farther north and is more zonally-expansive than the hot-to-cold whiplash, with positive geopotential height anomalies extending across the North Pacific Ocean and into northern Siberia (Figure 4.12a). This ridge does not persist through the whiplash event, and dissipates completely by lag days 4-6 (Figure 4.12d).

Additionally, prior to the HSD there is an anomalous trough over the northern US and Canada, which lifts and moves eastward into the Atlantic between days -2 and 0 (Figure 4.12c). The atmospheric pattern then transitions to positive geopotential height anomalies over the US Southern Plains, which can be linked with anomalous warmth that was experienced through the hydrostatic and hypsometric equations (Figures 4.12a and b). The warm anomalies originate from a ridge off the US west coast during days -5 to -3 (Figure 4.12a). It is possible that when the negative geopotential height anomalies undercut the Alaskan/North Pacific ridge, the ridge off the US west coast was forced south towards the southern US and Mexico (Figure 4.12c). Additionally, it may have been a shortwave ridge south of the amplified Alaskan ridge that weakened from the negative geopotential height anomalies to the west, before restrengthening slightly over land (Figure 4.12a and b). Or lastly, it may be a result of the relaxation of the blocking pattern, with the ridging originating over Mexico. Future analysis is needed to determine its origin.

The west coast ridge dissipates by days 1 to 3, although the presence of positive geopotential height anomalies still exist (Figure 4.12c). By days 4 to 6, the positive geopotential height anomalies move off the US east coast and into the Atlantic, and zonal flow remains over the central US (Figure 4.12d). Overall, the evolution of the tropospheric flow includes a dissipating North Pacific/Alaskan ridge, a deep trough propagating lifting and propagating into the Atlantic Ocean, and finally a transition to positive geopotential height anomalies over the Southern Plains (Figure 4.12). Reasons for the dissipating block could also be connected to the stratosphere.

4.2.2 Stratospheric Relationship and the Dissipating Block

As was previously discussed, the stratosphere can influence tropospheric flow, especially in the winter, so we also considered its impacts on cold-to-hot whiplash events. The 50-hPa flow pattern is very different from the hot-to-cold whiplash (Figure 4.2). For all the cold-to-hot 50-hPa composites (Figure 4.13), there are 3 statistically significant areas: a negative height anomaly in northern Canada and Greenland, a positive height anomaly in Siberia, and a positive height anomaly in northwestern Europe. This pattern sets up between days -5 to -3, and as it approaches the HSD the negative anomaly substantially intensifies, reaching its peak intensity during days -2 to 0 (Figure 4.13a and b). The SPV at 50-hPa appears relatively strong, with the presence of robust negative geopotential height anomalies near the core of the SPV. It appears somewhat stretched, meaning the negative geopotential height anomalies are located further south into Canada and the US prior to the HSD (Figure 4.13a and b). Following the HSD, the anomaly pattern persists through day 6, although the negative geopotential height anomaly recedes northward after the HSD, contracting the SPV and reducing the stretching (Figure 4.13c and d).

The 10-hPa composites (Figure 4.14) indicate similar findings to the 50-hPa composites. The negative height anomaly is still present in the same area as the 50-hPa composites (Figure 4.13). Additionally, positive height anomalies still exist over northern Asia and Europe, but prior to the HSD the positive height anomaly is enhanced over northeastern Russia, whereas following the HSD, the positive anomaly is amplified over northwestern Europe. The SPV strength is also anomalously stronger than at 50-hPa. Overall, the stratospheric composites suggest that there is a disturbed SPV during cold-to-hot whiplashes. While SPV stretching is present before the HSD, the SPV contracts following the HSD. This contraction suggests a stronger SPV in the later half of the whiplash event. To further examine SPV strength, we next investigate the weather regimes associated with cold-to-hot whiplashes.

4.2.3 Weather Regimes and Cold-to-Hot Whiplashes

We next look to link our cold-to-hot whiplash events with the North American winter weather regimes, as a way of exploring their SPV strength and inferring the potential for predictability of these events at extended lead times. Since the sample size for the cold-to-hot whiplashes is substantially less than the hot-to-cold whiplashes, breaking down the events by dominant regimes does not offer much benefit. Instead, we examine one heatmap with the evolution of the regimes through the whiplash events (Figure 4.15). Prior to the HSD, there are 3 dominant regimes: the AkR, the WCR, and the ArH, aligning with the regimes associated with central US CAOs in Millin et al. (2022) (Figure 4.15). With the exception of 2 events, the cold-to-hot whiplashes are in either an AkR or WCR regime -4 to -3 days before to the HSD. Additionally, following the HSD only 5 of the events remain in an AkR or WCR pattern, while the remaining transition to a mix of ArL, PT, or ArH (Figure 4.15). Three of the 4 events that

transition into AkR eventually transition into ArL or PT as well. The WCR regime is relatively similar to the AkR regime, and prior research indicates that the AkR regime is associated with the "morphology of the SPV" (Lee et al. 2019). However, both the PT and ArL are linked to a stronger SPV, indicating a transition to a stronger SPV following the HSD. This also aligns with Figures 4.13 and 4.14, which illustrate negative geopotential height anomalies in the area of the SPV, which would in turn strengthen the SPV. Overall, cold-to-hot whiplashes are associated with stronger SPVs.

In summary, while there are certain atmospheric circulation patterns present in both the hot-to-cold and cold-to-hot whiplashes, they have distinct evolutions. Hot-to-cold whiplashes are a result of an increase in atmospheric blocking and a stretched SPV, with possible influences from stratospheric wave reflection for about half of the events. In contrast, cold-to-hot whiplashes are characterized by the breakdown of a blocking pattern and an already amplified trough that lifts throughout the whiplash event. Positive geopotential height anomalies arise following its departure and persist through the end of the whiplash. The SPV states also vary between whiplash types. The hot-to-cold whiplash 50-hPa and 10-hPa geopotential height composites suggest a transition to a weaker SPV state and the North American winter weather regimes support that, with the dominant regimes suggesting a transition to a weaker SPV, or sustaining an already weak SPV. This is contrast to cold-to-hot whiplashes, which feature a transition to a stronger SPV regime, which are also evident from strong negative geopotential height anomalies in the corresponding 50-hPa and 10-hPa geopotential height composites. These distinctive patterns lead to vastly different precursors.

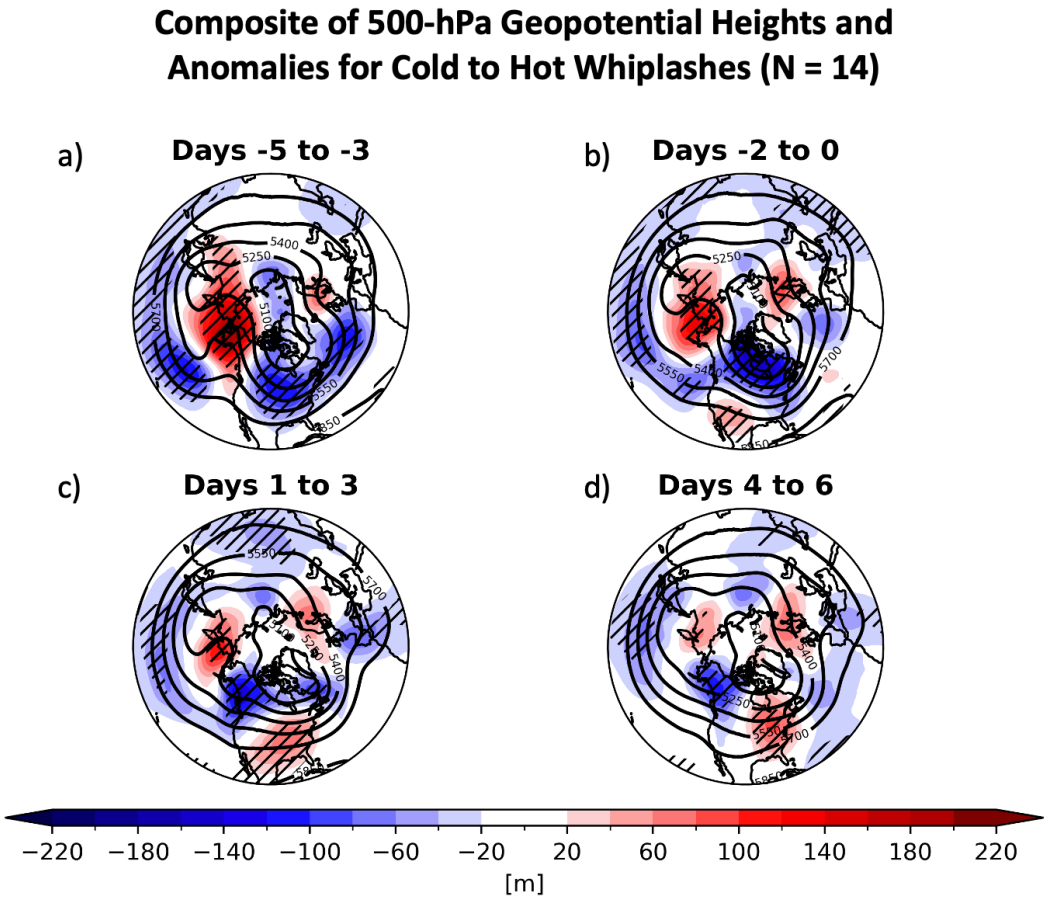

Figure 4.12: Lagged 500-hPa geopotential heights (meters; contours with an interval of 150m) and anomalies (meters; shading) for cold-to-hot whiplashes over lagged (a) days -5 to -3, (b) days -2 to 0 , (c) days 1 to 3, and (d) days 4 to 6 (N = 45). Hatching represents where anomalies are significant at the $p < 0.05$ level. Lag day 0 is the corresponding HSD.

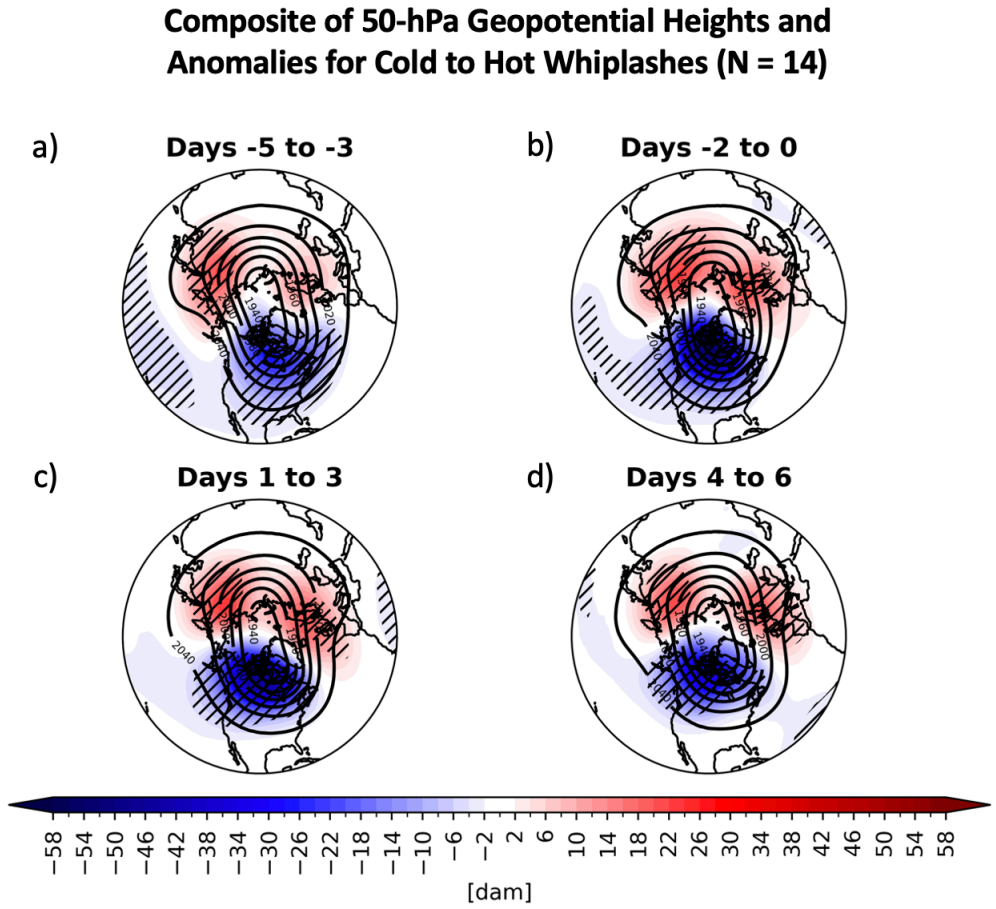

Figure 4.13: As in Fig. 4.12 but for 50-hPa geopotential heights and anomalies. Contour interval every 150m.

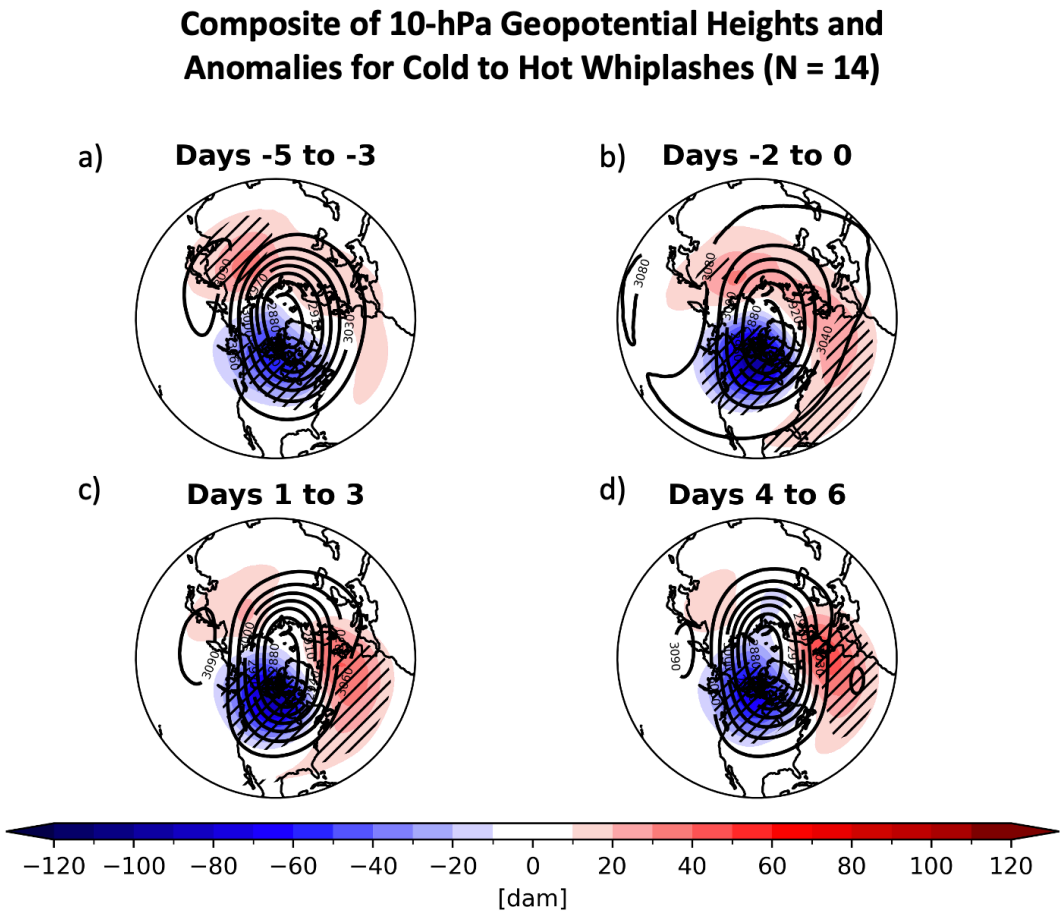

Figure 4.14: As in Fig. 4.12 but for 10-hPa geopotential heights and anomalies. Contour interval every 150m.

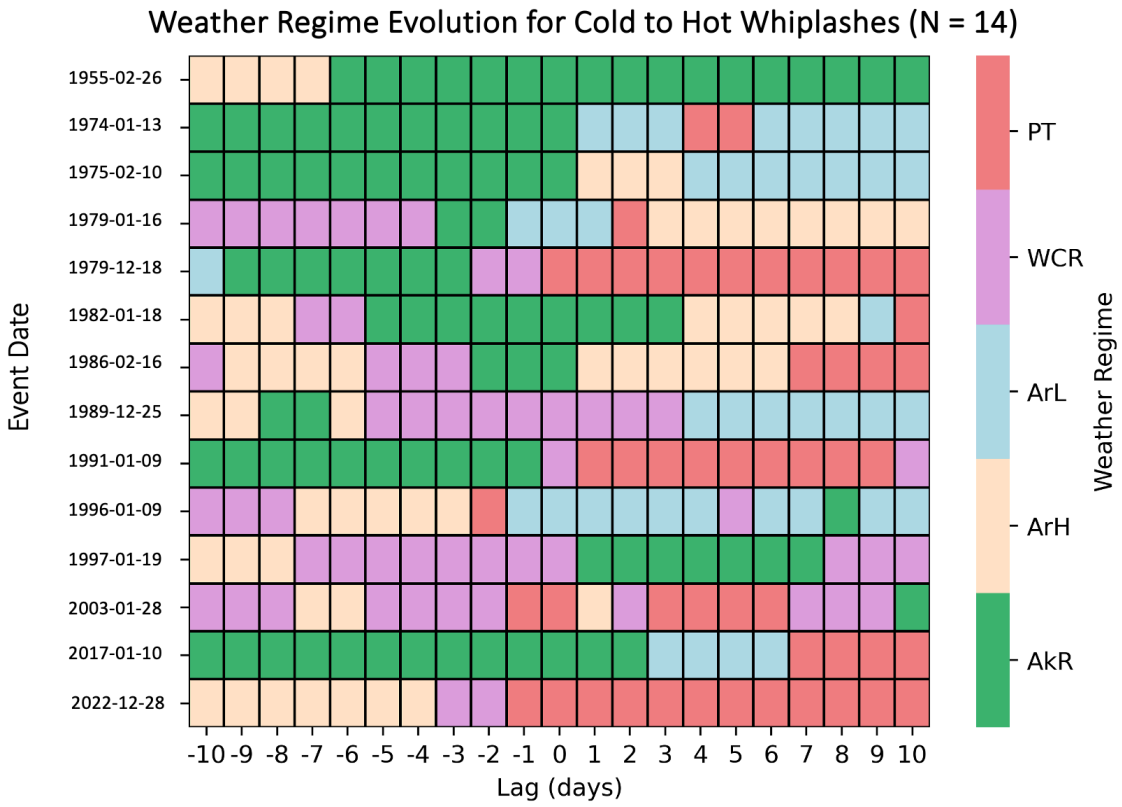

Figure 4.15: Lagged North American Winter Weather regimes for cold-to-hot whiplashes by event date (N = 14). Colors indicate different regimes. Event date on y-axis is each event's corresponding HSD.

Chapter 5

Discussion and Conclusions

Temperature whiplash events pose a threat the US Southern Plains, as temperature variability is projected to increase in a changing climate. This thesis aimed to define temperature whiplash over a regional domain to allow for enhanced adaptation to these extreme events. The new methodology presented can be applied to any domain by adjusting the location box, which is an advantage over other methodologies. Additionally, forecasting of the TSI was skillful when using the Geophysical Fluid Dynamics Laboratory's seasonal prediction system, which suggests that forecasting temperature whiplashes with this methodology, especially in the S2S time frame, could be relatively skillful as well (Yang et al. 2022). In addition to defining temperature whiplash, we also examined the characteristics and evolution of temperature whiplash events in the US Southern Plains, and suggested atmospheric connections that could be used to enhance S2S prediction.

We defined and examined two types of whiplashes in the US Southern Plains: hot-to-cold and cold-to-hot. Hot-to-cold whiplashes occur more frequently than cold-to-hot whiplashes, due to (a) more HSDs being hot-to-cold swings and (b) a higher percentage of them meeting the whiplash criteria. The number of HSDs and hot-to-cold temperature whiplashes have been increasing since the 2000s and 2010s respectively, highlighting the increased temperature variability in the mid-latitudes as mentioned in Cohen (2016) (Figure 3.3). Cold-to-hot whiplashes do not exhibit any substantial trends, and appear more sporadic. The most extreme HSDs (the top 5%) also illustrate

an increase in the 2020s, doubling the number of HSDs from the 2000s and 2010s already (Figure 3.4).

The atmospheric patterns associated with temperature whiplashes are whiplash-type dependent. While both whiplash types feature atmospheric blocking, hot-to-cold whiplashes exhibit an increase in blocking strength throughout the event, whereas cold-to-hot whiplashes feature a decaying block (Figures 4.1 and 4.12). The hot-to-cold whiplash block induces amplification of the downstream flow, leading to a deep, expansive trough over the central US (Figure 4.1). This trough's southward propagation is what leads to the cold spell in the hot-to-cold whiplash. Conversely, the cold-to-hot whiplash exhibits an already strong trough over most of the US, which subsequently lifts due to a relaxation of the atmospheric pattern as it propagates into the Atlantic Ocean (Figure 4.12).

The evolution of the 500-hPa geopotential height patterns can also be explained through North American winter weather regimes. The 3 regimes that categorize the hot-to-cold whiplashes on the HSD are the ArH, AkR, and ArL (Figure 4.8). The strength of the SPV also ties into these regimes and their relationship to temperature whiplash events (Lee et al. 2019; Charlton-Perez et al. 2018). In the ArH HSD regime, the evolution suggests an already weak or weakened SPV (Figure 4.9). However, the AkR and ArL HSD regimes are characteristic of a stronger than average SPV (Figures 4.10 and 4.11).

We also identified that the hot-to-cold whiplashes are related to troposphere-stratosphere interactions. Our results suggest that stratospheric wave reflection may be occurring in the 3 to 7 days prior to the HSD (Figure 4.7). However, this wave reflection is not as persistent as in Matthias and Kretschmer (2020) or Messori et al. (2022). This quick reflection supports the findings of Millin et al. (2022), which also found a shorter reflection period was associated with CAOs in the US Southern Plains. The shorter

reflection period may not provide a flux strong or persistent enough to reflect the wave over Canada. The different Canada and Siberia domains used to calculate the RI suggests the need for additional research into different reflection locations and their subsequent tropospheric impacts. These results also support Millin et al. (2022), which selected different reflection domains as well.

Cold-to-hot whiplashes, while they have large negative stratospheric geopotential height anomalies over North America (Figures 4.13 and 4.14), do not feature the same stratospheric connections as the hot-to-cold whiplashes. They transition into weather regimes associated with a stronger SPV, which is confirmed by the strong negative anomalies near the center of the SPV in Figures 4.13 and 4.14. Cold-to-hot whiplashes seem less predictable than hot-to-cold whiplashes, as they have a small sample size and no obvious trends in occurrence frequency or magnitude (Figures 3.13 and 3.14). The magnitude of the stratospheric anomalies are large, which may be a reason for the small sample size (Figures 4.13 and 4.14). It is possible that cold-to-hot temperature swings do not have temperature anomalies as strong or persistent as hot-to-cold swings, and therefore the whiplash criteria may be too limiting to adequately represent the significant societal impacts from cold-to-hot temperature swings. Future analysis includes exploring cold-to-hot whiplash precursors and addressing these questions.

We hypothesized that temperature whiplash events may have similar precursors to CAOs and winter warm spells, which was supported by our analyses; atmospheric blocking, elements of both CAOs and winter warm spells, and stratospheric wave reflection, a feature of US Southern Plains CAOs, were present in the temperature whiplash events. However, temperature whiplashes were not directly connected to climate modes like CAOs were. There were no statistically significant correlations between whiplash events and ENSO, the Arctic Oscillation, the North Atlantic Oscillation, and the Pacific-North American Pattern, although it is possible that these modes indirectly

affect whiplash frequency and magnitude through to their influence on local temperature variability. Additional analysis revealed a possible connection between cold-to-hot whiplashes and the NPO (not shown), but more research is needed. On a continental scale, Yang et al. (2022) found that the seasonal TSI could be connected to multiple climate modes. This suggests that while climate modes may be used to predict seasonal TSI over a large domain, smaller domains and smaller swing timescales may require different drivers, confirming our second hypothesis. Additionally, our study separated the temperature whiplashes into two types depending on their sign and anomalies. Future work includes separating the seasonal TSI in Yang et al. (2022) in this way to examine the different swing directions and their subsequent climate mode connections.

The results of this study support the conclusions in Francis et al. (2021), which found that in the winter, node 9, which strongly resembles the Alaskan ridge regime pattern (Millin et al. 2022) and our hot-to-cold whiplash composite (Figure 4.1b-d), had a significant increase in weather whiplashes when the dataset (from 1948-2019) was split into 2 20-year periods. While this study focused on the US Southern Plains domain, examining temperature whiplashes over other regions would be able to provide more context on regional precursors, and offer additional relevance to their S2S predictions.

As temperature whiplashes increase in the US Southern Plains, the threat to society persists. However, S2S predictability of extreme events, like temperature whiplashes, still remains a challenge. Through our analysis, we identified atmospheric patterns, specifically blocking and stratospheric wave reflection, that can be used in the S2S time frame to possibly improve S2S forecasts of temperature whiplashes, especially the hot-to-cold whiplashes. Ding et al. (2023) identifies wave reflection as a precursor to North American cold air events, which occur 5-25 days after strong wave reflection events. In addition, preliminary research has indicated that blocking has the ability to enhance

S2S predictions as well (Kautz et al. 2022; Quandt et al. 2017). Since temperature whiplash events can be connected to both phenomena, the potential to improve their S2S predictions is promising. In addition to these precursors, recent studies have identified additional factors to improve S2S forecasting of extreme temperature events, including capturing the importance of wave breaking (Millin and Furtado 2022) and the soil moisture-surface flux (Benson and Dirmeyer 2023), as well as using new techniques like machine learning (Kiefer et al. 2023).

In conclusion, this thesis offers a framework for future temperature whiplash studies, and emphasizes the need for future work to better anticipate extremes in the S2S range. By advancing our understanding and predictions of these extremes, we can better anticipate and improve resiliency of extreme temperature events.

Reference List

Amini, S., and D. M. Straus, 2019: Control of storminess over the Pacific and North America by circulation regimes. *Climate Dynamics*, **52 (7)**, 4749–4770, https://doi.org/10.1007/s00382-018-4409-7.

Baldwin, M. P., and T. J. Dunkerton, 2001: Stratospheric harbingers of anomalous weather regimes. *Science*, **294 (5542)**, 581–584, https://doi.org/10.1126/science.1063315.

Benson, D. O., and P. A. Dirmeyer, 2023: The soil moisture–surface flux relationship as a factor for extreme heat predictability in subseasonal to seasonal forecasts. *Journal of Climate*, **36 (18)**, 6375 – 6392, https://doi.org/10.1175/JCLI-D-22-0447.1.

Casson, N. J., and Coauthors, 2019: Winter weather whiplash: Impacts of meteorological events misaligned with natural and human systems in seasonally snow-covered regions. *Earth's Future*, **7 (12)**, 1434–1450, https://doi.org/10.1029/2019EF001224.

Cellitti, M. P., J. E. Walsh, R. M. Rauber, and D. H. Portis, 2006: Extreme cold air outbreaks over the united states, the polar vortex, and the large-scale circulation. *Journal of Geophysical Research: Atmospheres*, **111 (D2)**, https://doi.org/10.1029/2005JD006273.

Charlton, A. J., and L. M. Polvani, 2007: A new look at stratospheric sudden warmings. part i: climatology and modeling benchmarks. *Journal of Climate*, **20 (3)**, 449 – 469, https://doi.org/10.1175/JCLI3996.1.

Charlton-Perez, A. J., L. Ferranti, and R. W. Lee, 2018: The influence of the stratospheric state on north atlantic weather regimes. *Quarterly Journal of the Royal Meteorological Society*, **144 (713)**, 1140–1151, https://doi.org/10.1002/qj.3280.

Christy, J., R. Clarke, G. Gruza, J. Jouzel, M. Mann, J. Oerlemans, M. Salinger, and S.-W. Wang, 2001: Observed climate variability and change. *Climate change 2001: The scientific basis. Contribution of working group I to the third assessment report of the Intergovernmental Panel on Climate Change [Houghton, J.T., Y. Ding, D.J. Griggs, M. Noguer, P.J. van der Linden, X. Dai, K. Maskell, and C.A. Johnson (eds.)]*, Cambridge University Press.

Cohen, J., 2016: An observational analysis: Tropical relative to arctic influence on midlatitude weather in the era of arctic amplification. *Geophysical Research Letters*, **43 (10)**, 5287–5294, https://doi.org/10.1002/2016GL069102.

Cohen, J., L. Agel, M. Barlow, C. I. Garfinkel, and I. White, 2021: Linking arctic variability and change with extreme winter weather in the united states. *Science*, **373 (6559)**, 1116–1121, https://doi.org/10.1126/science.abi9167.

Cohen, J., and Coauthors, 2014: Recent Arctic amplification and extreme mid-latitude weather. *Nature Geoscience*, **7 (9)**, 627–637, https://doi.org/10.1038/ngeo2234.

Coughlan de Perez, E., and Coauthors, 2016: Action-based flood forecasting for triggering humanitarian action. *Hydrology and Earth System Sciences*, **20 (9)**, 3549–3560, https://doi.org/10.5194/hess-20-3549-2016.

Ding, X., G. Chen, P. Zhang, D. I. V. Domeisen, and C. Orbe, 2023: Extreme stratospheric wave activity as harbingers of cold events over North America. *Communications Earth & Environment*, **4 (1)**, 187, https://doi.org/10.1038/s43247-023-00845-y.

Domeisen, D. I. V., and Coauthors, 2023: Prediction and projection of heatwaves. *Nature Reviews Earth & Environment*, **4 (1)**, 36–50, https://doi.org/10.1038/s43017-022-00371-z.

Francis, J. A., W. Chan, D. J. Leathers, J. R. Miller, and D. E. Veron, 2009: Winter northern hemisphere weather patterns remember summer arctic sea-ice extent. *Geophysical Research Letters*, **36 (7)**, https://doi.org/doi.org/10.1029/2009GL037274.

Francis, J. A., N. Skific, S. J. Vavrus, and J. Cohen, 2021: Measuring "weather whiplash" events in North America: a new large-scale regime approach. Section: Atmospheric Sciences.

Francis, J. A., and S. J. Vavrus, 2012: Evidence linking arctic amplification to extreme weather in mid-latitudes. *Geophysical Research Letters*, **39 (6)**, https://doi.org/10.1029/2012GL051000.

Grace, T., K. Pegion, and J. B. Basara, 2024: Atmospheric and surface dynamics during winter warm spells in the southern great plains: insights from the 2021 case study. *JGR Atmospheres*.

Grise, K. M., S.-W. Son, and J. R. Gyakum, 2013: Intraseasonal and interannual variability in North American storm tracks and its relationship to equatorial Pacific variability. *Monthly Weather Review*, **141 (10)**, 3610–3625, https://doi.org/10.1175/MWR-D-12-00322.1.

Harnik, N., 2009: Observed stratospheric downward reflection and its relation to upward pulses of wave activity. *Journal of Geophysical Research: Atmospheres*, **114 (D8)**, https://doi.org/10.1029/2008JD010493.

Hersbach, H., and Coauthors, 2020: The era5 global reanalysis. *Quarterly Journal of the Royal Meteorological Society*, **146 (730)**, 1999–2049, https://doi.org/10.1002/qj.3803.

Higgins, R. W., A. Leetmaa, and V. E. Kousky, 2002: Relationships between climate variability and winter temperature extremes in the united states. *Journal of Climate*, **15 (13)**, 1555 – 1572, https://doi.org/10.1175/1520-0442(2002)015⟨1555:RBCVAW⟩2.0.CO;2.

IPCC, 2023: *Climate change 2021 – the physical science basis: working group I contribution to the sixth assessment report of the intergovernmental panel on climate change*, chap. Weather and climate extreme events in a changing climate, 1513–1766. Cambridge University Press.

Kautz, L.-A., O. Martius, S. Pfahl, J. G. Pinto, A. M. Ramos, P. M. Sousa, and T. Woollings, 2022: Atmospheric blocking and weather extremes over the euro-atlantic sector – a review. *Weather and Climate Dynamics*, **3 (1)**, 305–336, https://doi.org/10.5194/wcd-3-305-2022.

Kiefer, S. M., S. Lerch, P. Ludwig, and J. G. Pinto, 2023: Can machine learning models be a suitable tool for predicting central european cold winter weather on subseasonal to seasonal time scales? *Artificial Intelligence for the Earth Systems*, **2 (4)**, e230 020, https://doi.org/10.1175/AIES-D-23-0020.1.

Kodera, K., H. Mukougawa, and S. Itoh, 2008: Tropospheric impact of reflected planetary waves from the stratosphere. *Geophysical Research Letters*, **35 (16)**, https://doi.org/10.1029/2008GL034575.

Kretschmer, M., J. Cohen, V. Matthias, J. Runge, and D. Coumou, 2018: The different stratospheric influence on cold-extremes in Eurasia and North America. *npj Climate and Atmospheric Science*, **1 (1)**, 44–44, https://doi.org/10.1038/s41612-018-0054-4.

Lee, C. C., 2022: Weather whiplash: Trends in rapid temperature changes in a warming climate. *International Journal of Climatology*, **42 (8)**, 4214–4222, https://doi.org/10.1002/joc.7458.

Lee, S. H., J. C. Furtado, and A. J. Charlton-Perez, 2019: Wintertime north american weather regimes and the arctic stratospheric polar vortex. *Geophysical Research Letters*, **46 (24)**, 14 892–14 900, https://doi.org/10.1029/2019GL085592.

Lin, H., 2015: Subseasonal variability of North American wintertime surface air temperature. *Climate Dynamics*, **45 (5-6)**, 1137–1155, https://doi.org/10.1007/s00382-014-2363-6.

Lin, S., and Coauthors, 2021: The immediate effects of winter storms and power outages on multiple health outcomes and the time windows of vulnerability. *Environmental Research*, **196**, 110 924, https://doi.org/10.1016/j.envres.2021.110924.

Loikith, P. C., and A. J. Broccoli, 2012: Characteristics of observed atmospheric circulation patterns associated with temperature extremes over north america. *Journal of Climate*, **25 (20)**, 7266 – 7281, https://doi.org/10.1175/JCLI-D-11-00709.1.

Matthias, V., and M. Kretschmer, 2020: The influence of stratospheric wave reflection on North American cold spells. *Monthly Weather Review*, **148 (4)**, 1675–1690, https://doi.org/10.1175/MWR-D-19-0339.1.

McIntyre, M. E., and T. N. Palmer, 1983: Breaking planetary waves in the stratosphere. *Nature*, **305 (5935)**, 593–600, https://doi.org/10.1038/305593a0.

Meehl, G. A., C. Tebaldi, H. Teng, and T. C. Peterson, 2007: Current and future u.s. weather extremes and el niño. *Geophysical Research Letters*, **34 (20)**, https://doi.org/10.1029/2007GL031027.

Mesonet, O., 2024: Long term average graph. URL https://www.mesonet.org/index.php/past_data/mesonet_averages_graphs#series%5B%5D=nrmn%3Atair_av%3Acurrent%3AN%3A0%3A%23000000%3AN%3A1&series%5B%5D=nrmn%3Atair_mx%3Aaverage%3AN%3A5%3A%23990000%3AN%3A1&series%5B%5D=nrmn%3Atair_av%3Aaverage%3AN%3A5%3A%23006600%3AN%3A1&series%5B%5D=nrmn%3Atair_mn%3Aaverage%3AN%3A5%3A%23000066%3AN%3A1.

Messori, G., M. Kretschmer, S. H. Lee, and V. Wendt, 2022: Stratospheric downward wave reflection events modulate North American weather regimes and cold spells. *Weather and Climate Dynamics*, **3 (4)**, 1215–1236, https://doi.org/10.5194/wcd-3-1215-2022.

Millin, O. T., and J. C. Furtado, 2022: The role of wave breaking in the development and subseasonal forecasts of the february 2021 great plains cold air outbreak. *Geophysical Research Letters*, **49 (21)**, e2022GL100 835, https://doi.org/10.1029/2022GL100835.

Millin, O. T., J. C. Furtado, and J. B. Basara, 2022: Characteristics, evolution, and formation of cold air outbreaks in the great plains of the united states. *Journal of Climate*, **35 (14)**, 4585 – 4602, https://doi.org/10.1175/JCLI-D-21-0772.1.

Molina, M. J., J. H. Richter, A. A. Glanville, K. Dagon, J. Berner, A. Hu, and G. A. Meehl, 2023: Subseasonal representation and predictability of north american weather regimes using cluster analysis. *Artificial Intelligence for the Earth Systems*, **2 (2)**, e220 051, https://doi.org/10.1175/AIES-D-22-0051.1.

Moon, J.-Y., B. Wang, and K.-J. Ha, 2011: ENSO regulation of MJO teleconnection. *Climate Dynamics*, **37 (5)**, 1133–1149, https://doi.org/10.1007/s00382-010-0902-3.

News6, 2013: Freezing rain brings power outages in northeastern oklahoma. URL https://www.newson6.com/story/5e3636df2f69d76f62054c12/freezing-rain-brings-power-outages-in-northeastern-oklahoma.

NWS, 2013: The winter storm of december 20-22, 2013. URL https://www.weather.gov/oun/events-20131220.

Perlwitz, J., and N. Harnik, 2003: Observational evidence of a stratospheric influence on the troposphere by planetary wave reflection. *Journal of Climate*, **16 (18)**, 3011 – 3026, https://doi.org/10.1175/1520-0442(2003)016⟨3011:OEOASI⟩2.0.CO;2.

Plumb, R. A., 1985: On the three-dimensional propagation of stationary waves. *J. Atmos. Sci.*, **42**, 217–229.

Quandt, L.-A., J. H. Keller, O. Martius, and S. C. Jones, 2017: Forecast variability of the blocking system over russia in summer 2010 and its impact on surface conditions. *Weather and Forecasting*, **32 (1)**, 61 – 82, https://doi.org/10.1175/WAF-D-16-0065.1.

Robertson, A. W., and M. Ghil, 1999: Large-scale weather regimes and local climate over the western united states. *Journal of Climate*, **12 (6)**, 1796 – 1813, https://doi.org/10.1175/1520-0442(1999)012⟨1796:LSWRAL⟩2.0.CO;2.

Robertson, A. W., A. Kumar, M. Peña, and F. Vitart, 2015: Improving and promoting subseasonal to seasonal prediction. *Bulletin of the American Meteorological Society*, **96 (3)**, ES49 – ES53, https://doi.org/10.1175/BAMS-D-14-00139.1.

Shuangmei, M., and Z. Congwen, 2023: Subseasonal swing of cold and warm extremes between Eurasia and North America in winter of 2020/21: initiation and physical process. *Environmental Research Letters*, **18**, https://doi.org/10.1088/1748-9326/acaabf.

Thompson, D. W. J., and J. M. Wallace, 2000: Annular modes in the extratropical circulation. part i: Month-to-month variability. *Journal of Climate*, **13 (5)**, 1000 – 1016, https://doi.org/10.1175/1520-0442(2000)013⟨1000:AMITEC⟩2.0.CO;2.

Tomczyk, A. M., A. Sulikowska, E. Bednorz, and M. Półrolniczak, 2019: Atmospheric circulation conditions during winter warm spells in central europe. *Natural Hazards*, **96**, 1413–1428, https://doi.org/10.1007/s11069-019-03621-4.

Vitart, F., and A. W. Robertson, 2018: The sub-seasonal to seasonal prediction project (S2S) and the prediction of extreme events. *npj Climate and Atmospheric Science*, **1 (1)**, 3, https://doi.org/10.1038/s41612-018-0013-0.

Westby, R. M., and R. X. Black, 2015: Development of anomalous temperature regimes over the southeastern united states: synoptic behavior and role of low-frequency modes. *Weather and Forecasting*, **30 (3)**, 553 – 570, https://doi.org/10.1175/WAF-D-14-00093.1.

Xie, Z., R. Black, and Y. Deng, 2017: The structure and large-scale organization of extreme cold waves over the conterminous united states. *Climate Dyn.*, **49**, 4075–4088, https://doi.org/10.1007/s00382-017-3564-6.

Yang, X., T. L. Delworth, L. Jia, N. C. Johnson, F. Lu, and C. McHugh, 2022: On the seasonal prediction and predictability of winter surface Temperature Swing Index over North America. *Frontiers in Climate*, **4**, https://doi.org/10.3389/fclim.2022.972119.

Yang, X., L. Jia, S. B. Kapnick, T. L. Delworth, G. A. Vecchi, R. Gudgel, S. Underwood, and F. Zeng, 2018: On the seasonal prediction of the western United States El Niño precipitation pattern during the 2015/16 winter. *Climate Dynamics*, **51 (9)**, 3765–3783, https://doi.org/10.1007/s00382-018-4109-3.

Yang, X., and Coauthors, 2015: Seasonal predictability of extratropical storm tracks in gfdl's high-resolution climate prediction model. *Journal of Climate*, **28 (9)**, 3592 – 3611, https://doi.org/10.1175/JCLI-D-14-00517.1.

Zheng, C., E. K.-M. Chang, H. Kim, M. Zhang, and W. Wang, 2021: Subseasonal prediction of wintertime northern hemisphere extratropical cyclone activity by subx and s2s models. *Weather and Forecasting*, **36 (1)**, 75 – 89, https://doi.org/10.1175/WAF-D-20-0157.1.

Zheng, C., E. K.-M. Chang, H.-M. Kim, M. Zhang, and W. Wang, 2018: Impacts of the madden–julian oscillation on storm-track activity, surface air temperature, and precipitation over north america. *Journal of Climate*, **31 (15)**, 6113 – 6134, https://doi.org/10.1175/JCLI-D-17-0534.1.